

# Pentanuclear Lanthanide Mono-organophosphates: Synthesis, Structure and Magnetism

Sandeep K. Gupta<sup>†</sup>, Stuart K. Langley<sup>‡</sup>, Kamna Sharma<sup>†</sup>, Keith S. Murray<sup>‡</sup> and Ramaswamy Murugavel<sup>†\*</sup>

<sup>†</sup> Department of Chemistry, Indian Institute of Technology Bombay, Powai, Mumbai, India.

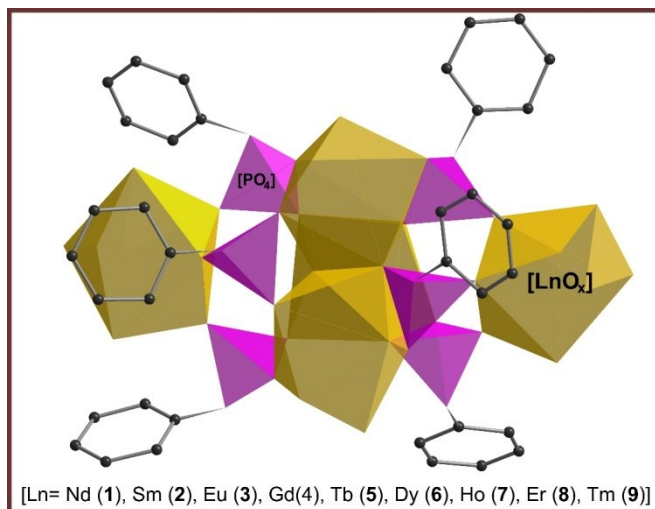
<sup>‡</sup> School of Science and the Environment, Division of Chemistry, Manchester Metropolitan University, Manchester, UK.

<sup>‡</sup> School of Chemistry, Monash University, Clayton, Victoria 3800, Australia.

**KEYWORDS:** Lanthanide organophosphates, magnetism, mono-ester of phosphoric acid, lanthanide contraction, pentanuclear clusters

*Supporting Information Placeholder*

**ABSTRACT:** Research on rare-earth phosphates has recently received substantial interest because of their unique physical and chemical properties. In recent years, because of their low solubility, research interest has been built on developing methodologies to prepare nanostructures and grow single crystals of inorganic rare-earth phosphates. The chemistry of rare-earth organophosphates, however is still at a latent stage. Contrary to the traditional hydrothermal route, we report rare examples of the synthesis of discrete pentanuclear lanthanide (III) organophosphate clusters assembled from a sterically encumbered mono-ester of phosphoric acid under mild reaction conditions. Single crystal X-ray analysis reveals that all the compounds possess a similar core structure  $[\text{Ln}_5(\mu_3\text{-OH})(\text{dipp})_6(\text{CH}_3\text{OH})_x(\text{H}_2\text{O})_y]^{2+}$  [Ln= Nd (1), Sm (2), Eu (3), Gd (4), Tb (5), Dy (6), Ho (7), Er (8), Tm (9)], where the charge balance is maintained by the presence of chelating nitrate anions, protonated tmeda, or  $\text{dipp}^{2-}$  ligands. The vacant coordination sites on the metal ions are satisfied by coordinated methanol or water molecules. The core structure of these clusters is built on a  $[\text{Ln}_3(\mu_3\text{-OH})(\text{dipp})_6]$  triangle where the phosphate ligands bridge to two further Ln(III) ions. The complexes display lanthanide contraction along the series, with Ln(III) ions displaying different coordination environments/geometries as we move along the series. All the compounds have been characterized by both analytical and spectroscopic techniques. Magnetic studies reveal the presence of weak antiferromagnetic magnetic exchange through the bridging  $\mu_3$ -hydroxo moiety and organophosphate groups for the  $\{\text{Gd}^{\text{III}}\}$  analogue, with a significant magnetic entropy change ( $25.8 \text{ J kg}^{-1} \text{ K}^{-1}$ ,  $\Delta H = 7 \text{ T}$ ). The anisotropic complexes reveal an absence of slow relaxation of magnetization, except for Nd (1), Dy (6) and Er (8) which show slow relaxation in an applied DC field.



## Introduction

Lanthanide coordination complexes have attracted great interest in the recent past owing to their potential applications in a wide variety of areas such as gas adsorption,<sup>1</sup> catalysis,<sup>2</sup> luminescence,<sup>3</sup> magnetic resonance imaging,<sup>4</sup> sensors,<sup>5</sup> etc. Recently there has been a huge thrust in the chemistry of rare earth complexes in view of the interesting single molecule magnet (SMM) behavior arising from the inherently large single-ion magnetic anisotropy and large ground spin state of several lanthanide ions.<sup>6,7</sup> Furthermore,

isotropic gadolinium complexes have been investigated for their potential application as molecular coolants in the field of magnetic refrigeration.<sup>8</sup> Although numerous ligands such as carboxylates, Schiff bases,  $\beta$ -ketonates, hydrazine, amine polyalcohol, macrocycles, etc. have been employed for the synthesis of rare earth complexes, the coordination chemistry of organophosphates is still to be well explored.

Research on rare-earth inorganic phosphates ( $\text{LnPO}_4$ ) have been reported in recent times highlighting the capability of this class of materials for applications in diverse fields.<sup>9</sup> This class of material possesses some remarkable

properties such as high thermal<sup>10</sup> and chemical stability<sup>11</sup>, low thermal conductivity<sup>12</sup>, high refractive index,<sup>13</sup> low water solubility<sup>14</sup> and hydrophobicity<sup>15</sup> among others. These unique features have led to the utilization of  $\text{LnPO}_4$  in a variety of applications such as ceramics,<sup>9d, 16</sup> catalysis,<sup>17</sup> and proton conductors.<sup>18</sup> Further,  $\text{LnPO}_4$  has been used as a host matrix for doping with other members of the family to reveal more interesting properties such as phosphors.<sup>19</sup> However, the low solubility of these materials prevent smooth crystallization and thus different methods have been reported to prepare single crystals of  $\text{LnPO}_4$ , most recently being the stringent solvothermal route.<sup>20</sup> One alternate method for the preparation of single crystals of lanthanide phosphates is to use the organic derivatives or esters of *ortho*-phosphoric acid, which aid the solubility in organic solvents and hinder fast nucleation. However, research on discrete lanthanide ion complexes derived from mono-esters of *ortho*-phosphoric acid are relatively unknown, although the chemistry of organophosphate ligands with transition metals has been well established.<sup>21,22,23</sup> While organophosphates (e.g. tri-*tert*-butyl phosphate) have been used in the past for the extraction of lanthanides and actinides ions,<sup>24</sup> only in very rare instances has the crystallographic structures of polymeric lanthanide organophosphate (di- or tri-esters)<sup>25</sup> or discrete actinide complexes<sup>26</sup> been established. This is due to the fact that lanthanide phosphates have very low solubility products, impeding the structural characterization of this type of material.<sup>14</sup>

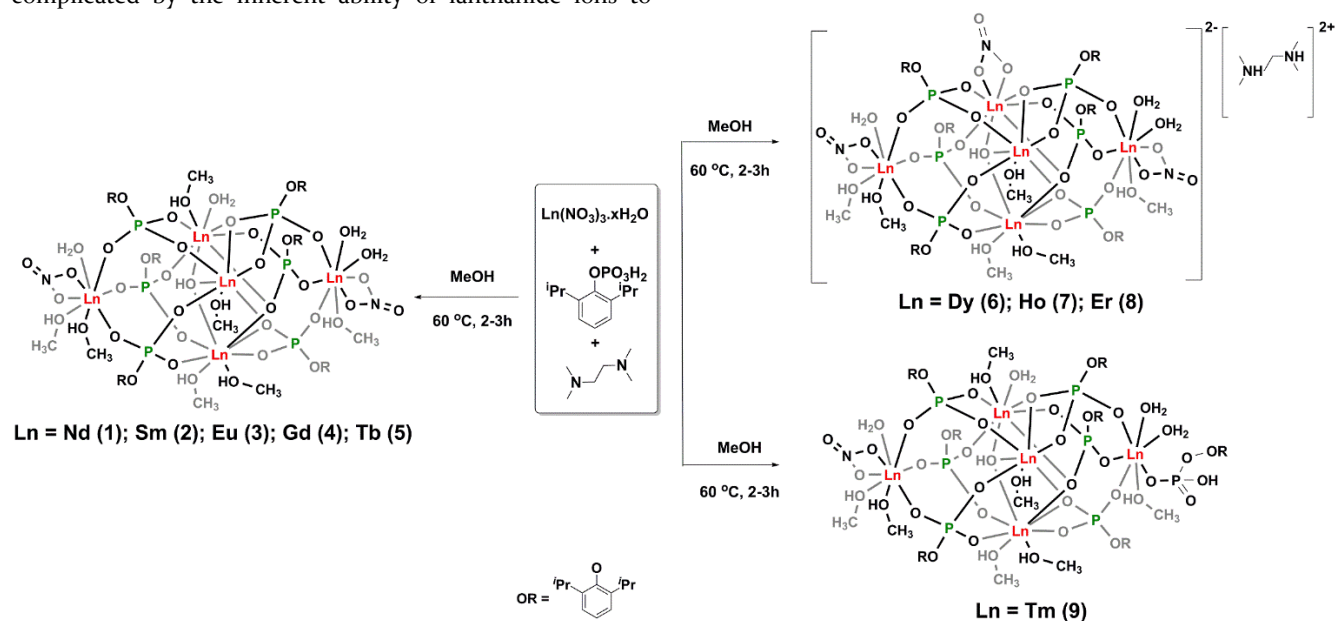
Examples of 4f and 3d-4f complexes of organophosphonates (structural analogue to organophosphates) exhibiting various metallic topologies have recently been reported with some of these clusters exhibiting interesting magnetocaloric effects behaving as molecular magnetic coolants.<sup>27</sup> In lanthanide phosphonate chemistry stringent solvothermal routes are often employed for the synthesis and growth of single crystals.<sup>27</sup> However in the case of organophosphate esters, the situation is more complicated by the inherent ability of lanthanide ions to

hydrolyze and cleave the ester P-O bonds leading to the formation of insoluble inorganic phosphates.<sup>28</sup> Interestingly, metal ions have also been reported to cleave the P-C bond in the case of organophosphonates during the solvothermal reaction conditions.<sup>29</sup> Thus, in order to prevent hydrolysis in the course of the reaction, we have precisely selected a sterically encumbered mono-ester of phosphoric acid - 2,6-di-*iso*-propylphenyl phosphate ( $\text{dippH}_2$ ), where the *isopropyl* group imparts additional solubility and provides a protective hydrophobic pocket near the hydrolytically susceptible -P-O bond of the ester. A preliminary account of this study, describing the isotropic Gd(III) derivative and its interesting magnetocaloric effect property has recently been reported.<sup>8f</sup> Building on our earlier efforts, the synthesis, structural characterization and investigation of the magnetic properties of an extended series of discrete polynuclear lanthanide complexes using the mono-ester of phosphoric acid namely  $\text{dippH}_2$  are reported.

## Results and discussion

### Synthetic aspects

The synthesis of lanthanide organophosphates was carried out under mild reaction conditions under an ambient aerobic atmosphere. Tetramethylethylene diamine (tmeda) was employed as the base for the deprotonation of the -P-OH groups of the phosphate ligand,  $\text{dippH}_2$ . The reaction of  $\text{Ln}(\text{NO}_3)_3 \cdot x\text{H}_2\text{O}$ , with  $\text{dippH}_2$  in the presence of tmeda (1:1:2 molar ratio) in a methanolic solution at 60 °C, leads to the formation of a family of pentanuclear lanthanide(III) phosphates [ $\text{Ln} = \text{Nd}$  (1),  $\text{Sm}$  (2),  $\text{Eu}$  (3),  $\text{Gd}$  (4),  $\text{Tb}$  (5),  $\text{Dy}$  (6),  $\text{Ho}$  (7),  $\text{Er}$  (8),  $\text{Tm}$  (9)] in quantitative yield (Scheme 1). Although the basic metal ion architecture is essentially same, small differences on the peripheral ligands result in the isolation of three unique structures as shown in Scheme 1.



**Scheme 1.** Synthesis of pentanuclear lanthanide phosphates (1-9).

Single crystals of each complex were obtained via slow evaporation of the solvent. In order to obtain pure

products, the reaction mixture kept for crystallization was repeatedly filtered until no precipitation was observed during

the evaporation. The compounds were obtained as block shaped crystals from the reaction mixture in one to two weeks. The molecular structures of all the clusters have been established by single crystal X-ray diffraction studies. All the new compounds have been characterized by means of both spectroscopic and analytical techniques. The molecular composition of the compounds deduced are listed in Table 1.

**Table 1.** Molecular composition of the pentanuclear lanthanide phosphates (**1-9**).

No	Molecular composition of single crystal
1	$[\text{Nd}_5(\mu_3\text{-OH})(\text{NO}_3)_2(\text{dipp})_6(\text{CH}_3\text{OH})_7(\text{H}_2\text{O})_4] \cdot 4\text{CH}_3\text{OH} \cdot \text{H}_2\text{O}$
2	$[\text{Sm}_5(\mu_3\text{-OH})(\text{NO}_3)_2(\text{dipp})_6(\text{CH}_3\text{OH})_7(\text{H}_2\text{O})_4] \cdot 5\text{CH}_3\text{OH}$
3	$[\text{Eu}_5(\mu_3\text{-OH})(\text{NO}_3)_2(\text{dipp})_6(\text{CH}_3\text{OH})_7(\text{H}_2\text{O})_4] \cdot 5\text{CH}_3\text{OH}$
4	$[\text{Gd}_5(\mu_3\text{-OH})(\text{NO}_3)_2(\text{dipp})_6(\text{CH}_3\text{OH})_7(\text{H}_2\text{O})_4] \cdot 5\text{CH}_3\text{OH}^{\text{8f}}$
5	$[\text{Tb}_5(\mu_3\text{-OH})(\text{NO}_3)_2(\text{dipp})_6(\text{CH}_3\text{OH})_7(\text{H}_2\text{O})_4] \cdot 4\text{CH}_3\text{OH} \cdot \text{H}_2\text{O}$
6	$[\text{Dy}_5(\mu_3\text{-OH})(\text{NO}_3)_2(\text{dipp})_6(\text{CH}_3\text{OH})_5(\text{H}_2\text{O})_2][\text{tmedaH}_2]_{0.5} \cdot 5\text{CH}_3\text{OH} \cdot 2\text{H}_2\text{O}$
7	$[\text{Ho}_5(\mu_3\text{-OH})(\text{NO}_3)_2(\text{dipp})_6(\text{CH}_3\text{OH})_5(\text{H}_2\text{O})_2][\text{tmedaH}_2]_{0.5} \cdot 5\text{CH}_3\text{OH} \cdot 2\text{H}_2\text{O}$
8	$[\text{Er}_5(\mu_3\text{-OH})(\text{NO}_3)_2(\text{dipp})_6(\text{CH}_3\text{OH})_5(\text{H}_2\text{O})_2][\text{tmedaH}_2]_{0.5} \cdot 5\text{CH}_3\text{OH} \cdot 2\text{H}_2\text{O}$
9	$[\text{Tm}_5(\mu_3\text{-OH})(\text{dipp})_7(\text{CH}_3\text{OH})_7(\text{H}_2\text{O})_3] \cdot 5\text{CH}_3\text{OH} \cdot 3\text{H}_2\text{O}$

### FTIR spectroscopy and thermogravimetric analysis

The FTIR spectra of compounds **1-9** were recorded as transparent discs that were diluted with KBr. Compounds **1-9** don't show a broad absorption band at  $\sim 2300\text{ cm}^{-1}$  in the infrared spectra indicating complete deprotonation of the phosphate ligands and hence the absence of any free P–OH groups in the molecular structure (Figure S1). The strong absorption for the P=O stretching vibrations and the symmetric and anti-symmetric M–O–P stretching vibrations are observed in the region  $1100$  and  $1050\text{-}950\text{ cm}^{-1}$ , respectively (see experimental section for details).

The stability of **1-9** has been analyzed by thermal decomposition analysis under an  $\text{N}_2$  atmosphere at a heating rate of  $10\text{ }^\circ\text{C min}^{-1}$ . All compounds reveal a similar type of weight loss (Figures S2). The first weight loss of about 10 % of the sample weight, up to  $200\text{ }^\circ\text{C}$ , is due to successive losses of lattice and coordinated solvent molecules. On further heating the sample up to  $500\text{ }^\circ\text{C}$ , there is loss of about 35-40 % of the total mass corresponding to the loss of most of the organic groups of the molecule. No major weight loss was observed between  $500\text{ }^\circ\text{C}$  and  $800\text{ }^\circ\text{C}$ .

### Structural features of lanthanide organophosphates

Single crystal X-ray diffraction analysis reveals that compounds **1-9** each display similar metal ion core architectures, built on a central triangle,  $[\text{Ln}_3(\mu_3\text{-OH})(\text{dipp})_6]$ , where the three Ln(III) ions are bridged by a  $\mu_3$ -hydroxo anion. The phosphate dianion embraces the central  $\text{Ln}_3(\mu_3\text{-OH})$  unit, forming a bridge from the triangle to the two peripheral lanthanide cations. The charge balance of each complex is maintained by the presence of chelating nitrate ions (**1-8**), protonated tmeda (**6-8**) and a terminal dipp<sup>2-</sup> ligand (**9**), the vacant coordination sites on the metal ions are satisfied by coordinated methanol or water molecules. Compounds **1-8** crystallize in the triclinic space group,  $P\bar{1}$ , while the thulium complex (**9**) crystallizes in the monoclinic space group,  $P2_1/n$ . A summary of the crystallographic refinement details is presented in Table 5 and 6. There are three distinct coordination environments found for this family of compounds, namely, **1-5**, **6-8** and **9**, respectively. Representative compounds, viz. **1** ( $\text{Nd}^{\text{III}}$ ), **6** ( $\text{Dy}^{\text{III}}$ ) and **9** ( $\text{Tm}^{\text{III}}$ )

are described in detail. The molecular structure of **4** has been described before.<sup>8f</sup> Compound **1** and **5** differ from **2**, **3** and **4** only by a replacement of lattice methanol solvate by water molecule (compounds (**1** and **5**); (**2**, **3** and **4**); (**6**, **7** and **8**) are isomorphous).

### Molecular structures of 1-5

Compounds **1-5** reveal an identical metal ion arrangement and coordination environment. All crystallize in the triclinic space group,  $P\bar{1}$ . Compound **1** will be described in detail. The asymmetric part of the unit cell in **1** contains five metal ions, six phosphate ligands, one  $\mu_3$ -OH and two nitrate groups at the core with coordinated methanol (seven) and water (four) molecules. In addition to this, there are four methanol and a water molecule in the crystal lattice. A perspective view of the molecular structure of **1** is shown in Figure 1. Complex **1** is therefore a discrete pentanuclear lanthanide organophosphate complex, enclosed by an organic sheath of aromatic rings around the periphery (Figure 2). Compound **1** contains a  $\mu_3$ -OH centered metal trinuclear unit,  $[\text{Nd}_3(\mu_3\text{-OH})(\text{dipp})_6]$ , where the three metal centers are bridged by the six phosphate ligands (Figure 3), which embrace two more metal centers at the periphery of the cluster to complete the pentanuclear trigonal bipyramidal construct (Figure 1). The average metal-oxygen distance in the trinuclear unit  $[\text{Nd}_3(\mu_3\text{-OH})]$  is  $2.463\text{ \AA}$ , whereas the average metal-metal distance is  $4.017\text{ \AA}$ . The distance of O25 from the mean plane of Nd1, Nd2, Nd3 is  $0.832\text{ \AA}$ . The angles around the  $\mu_3$ -OH oxygen atom with the metal centres are  $\text{Nd3-O25-Nd2} \dots 109.63(2)^\circ$ ,  $\text{Nd3-O25-Nd1} \dots 108.96(2)^\circ$  and  $\text{Nd2-O25-Nd1} \dots 109.03(2)^\circ$ . The core structure of the metal trinuclear unit,  $[\text{Nd}_3(\mu_3\text{-OH})(\text{dipp})_6]$  resembles the  $[\text{Ln}(\mu_3\text{-OH})_4]$  cubane structure with the absence of one Ln(III) ion, as observed in other lanthanide complexes (Figure 3).<sup>8g, 30</sup>

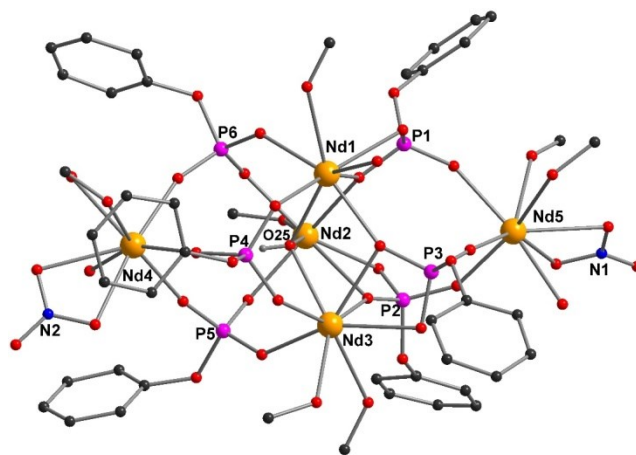


**Figure 1.** Molecular structure of the pentanuclear neodymium organophosphate, **1**. Isopropyl groups, lattice solvates and most hydrogen atoms are removed for clarity.

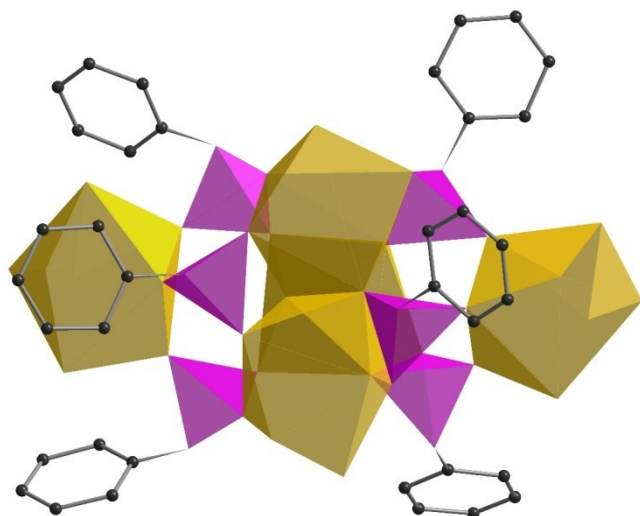


**Figure 2.** Polyhedral diagram showing the inorganic core wrapped within the organic part of the phosphate ligands in **1**. Yellow and pink polyhedra represent the coordination environment of the Nd(III) ions and phosphorous atom, respectively.

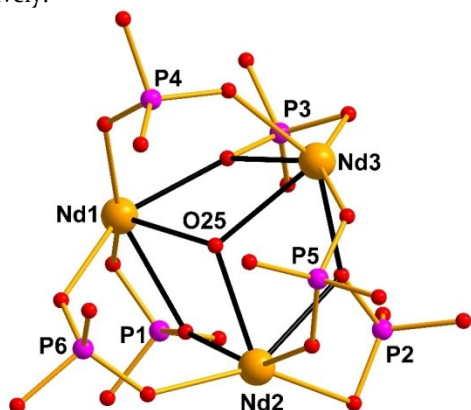


**Figure 3.** View of the  $[\text{Nd}_3(\mu_3\text{-OH})(\text{dipp})_6]$  triangle for **1**. The organic part of the phosphate ligands has been removed for clarity.

Of the six phosphate ligands that are present there are two sets of three phosphates, each that bind to the Ln(III)-ions in a  $[3.111]$  and  $[3.211]$  fashion, respectively (Figure 4).<sup>31</sup> Phosphates P1, P2 and P3 bind, through the O-atoms in the  $[3.211]$  fashion on one side of the complex, bridging Nd1, Nd2 and Nd3 with the peripheral Nd5 ion. Phosphates P4, P5 and P6 bind in the  $[3.111]$  fashion on the other side of the complex, bridging Nd1, Nd2 and Nd3 with Nd4. The metal-metal distances between the terminal and the central neodymium ions vary in the range of 5.467–5.838 Å. The metal-metal distance between the two peripheral neodymium ions is 10.266(2) Å. The two nitrate anions chelate to the peripheral Nd4 and Nd5 ions. The coordination spheres of the central and outer neodymium ions are completed by coordinated solvent (MeOH and H<sub>2</sub>O) molecules. Four of the neodymium atoms (Nd1, Nd3, Nd4, Nd5) are eight coordinate, whereas Nd2 is seven coordinate. The coordination environment around the rare-earth metal ions were analyzed by SHAPE 2.1 software<sup>32</sup> (Table S17 and S18). The  $\{\text{NdO}_8\}$  environment built around Nd1, Nd3 and Nd5 shows least deviation from the ideal  $C_{2v}$  symmetry occupying a distorted biaugmented trigonal

prism geometry, the  $\{\text{NdO}_8\}$  environment around Nd4 shows least deviation from the ideal  $D_{2d}$  symmetry adopting a triangular dodecahedron geometry (Figure 5). The  $\{\text{NdO}_7\}$  environment around Nd2 displays a capped trigonal prismatic geometry with least deviation from the ideal  $C_{2v}$  symmetry (Figure 5).

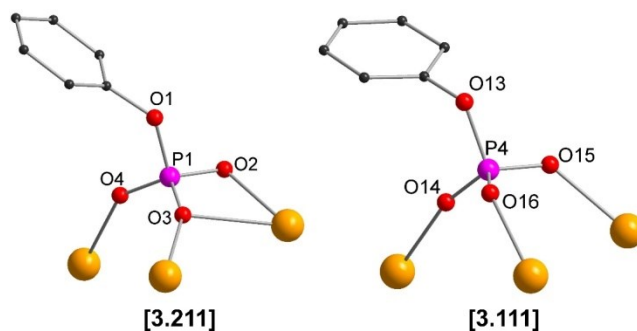


**Figure 4.** Binding mode of the phosphate ligands in **1**.

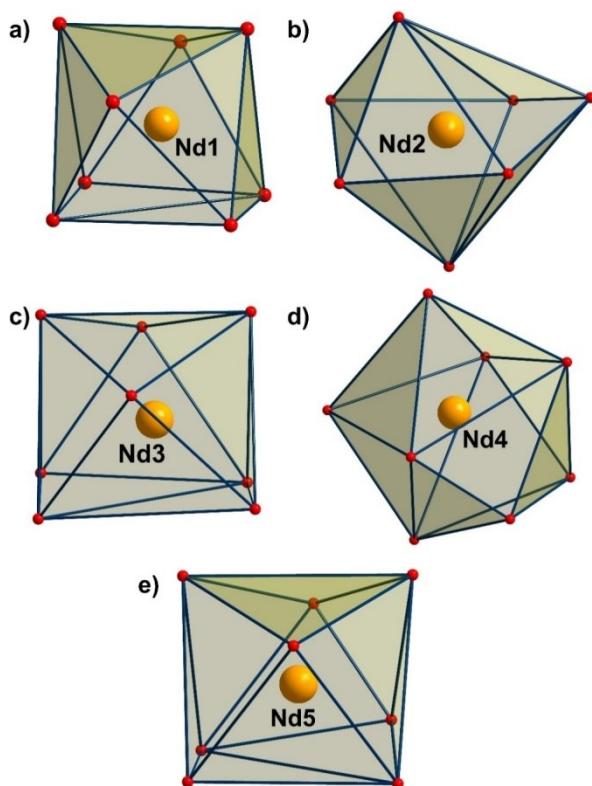


**Figure 5 (a-e).** Polyhedral representation of the distorted coordination geometry around the Nd(III) ions in the crystal structure of compound **1**.

Along with the coordinated and lattice solvent molecules, the coordinated nitrate ions are involved in extensive intermolecular and intramolecular H-bonding, leading to the formation of two-dimensional self-assembled hydrogen bonded networks of the pentanuclear complexes (Figure 6).

The structural features of **2-4** are similar to those of **1**, with the metal ions displaying similar coordination environments (Table S2-S4). As we move along the series it is observed that the Ln-O25 and Ln...Ln distances in the central triangular unit gradually decrease (Table 2).

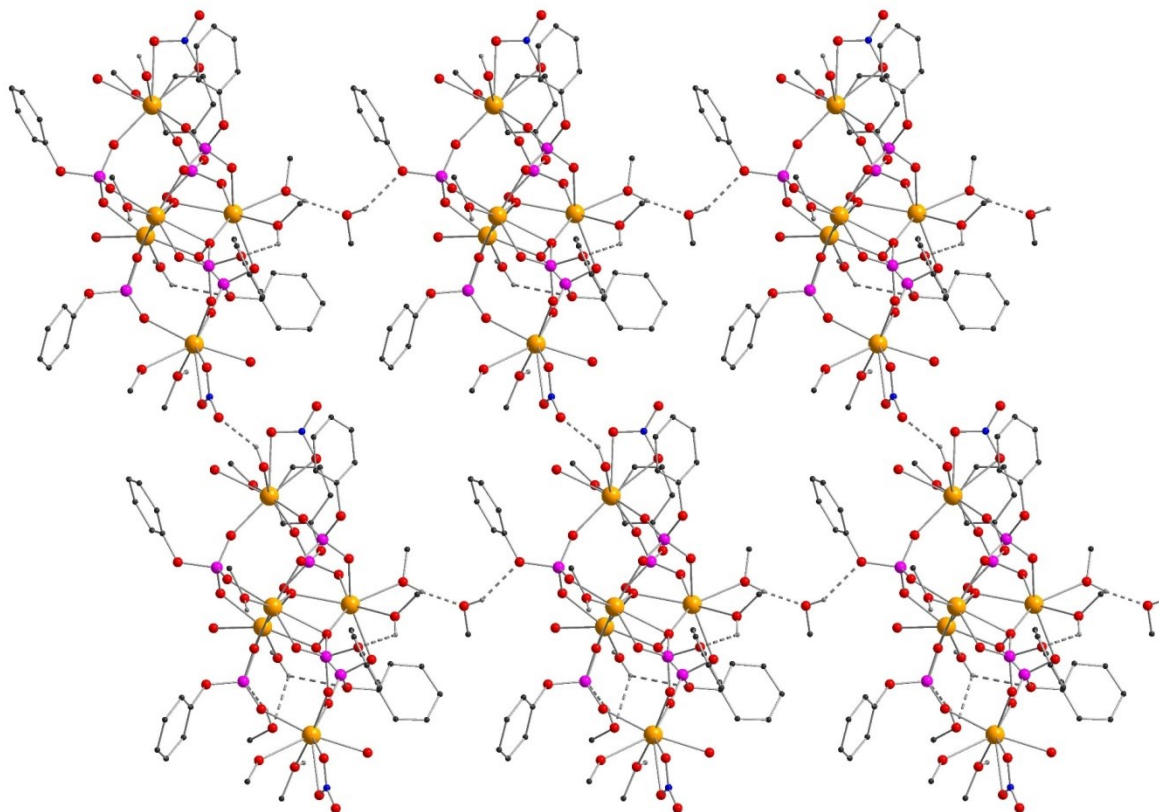


**Figure 6.** Intermolecular and intramolecular H-bonding in **1** leading to the formation of two-dimensional hydrogen bonded networks of the pentanuclear rare-earth phosphate complexes.

**Table 2.** Ln-O25 and Ln...Ln distances (Å) in the central triangular unit [Ln<sub>3</sub>(μ<sub>3</sub>-OH)(dipp)<sub>6</sub>] in 1-9.

1		2		3	
Nd1-O25	2.455(4)	Sm1-O25	2.421(4)	Eu1-O25	2.403(3)
Nd2-O25	2.437(4)	Sm2-O25	2.403(4)	Eu2-O25	2.393(3)
Nd3-O25	2.499(4)	Sm3-O25	2.474(4)	Eu3-O25	2.456(3)
Nd1-Nd2	3.998(7)	Sm1-Sm2	3.927(7)	Eu1-Eu2	3.905(8)
Nd1-Nd3	4.034(6)	Sm1-Sm3	3.979(6)	Eu1-Eu3	3.956(7)
Nd2-Nd3	4.018(6)	Sm2-Sm3	3.965(6)	Eu2-Eu3	3.942(7)
Nd1-O25-Nd2	109.64(1)	Sm1-O25-Sm2	109.00(2)	Eu1-O25-Eu2	109.05(1)
Nd1-O25-Nd3	109.03(1)	Sm1-O25-Sm3	108.71(1)	Eu1-O25-Eu3	109.03(1)
Nd2-O25-Nd3	108.96(1)	Sm2-O25-Sm3	108.75(2)	Eu2-O25-Eu3	108.77(1)
4		5		6	
Gd1-O25	2.398(5)	Tb1-O25	2.400(4)	Dy1-O25	2.365(3)
Gd2-O25	2.375(5)	Tb2-O25	2.363(4)	Dy2-O25	2.340(3)
Gd3-O25	2.448(5)	Tb3-O25	2.438(4)	Dy3-O25	2.390(3)
Gd1-Gd2	3.886(8)	Tb1-Tb2	3.870(7)	Dy1-Dy2	3.820(5)
Gd1-Gd3	3.940(9)	Tb1-Tb3	3.930(6)	Dy1-Dy3	3.900(5)
Gd2-Gd3	3.919(8)	Tb2-Tb3	3.898(6)	Dy2-Dy3	3.852(4)
Gd2-O25-Gd1	109.02(2)	Tb1-O25-Tb2	108.68(1)	Dy1-O25-Dy2	108.59(1)
Gd2-O25-Gd3	108.70(2)	Tb1-O25-Tb3	108.64(1)	Dy1-O25-Dy3	110.21(1)
Gd1-O25-Gd3	108.79(2)	Tb2-O25-Tb3	108.58(1)	Dy2-O25-Dy3	109.05(1)
7		8		9	
Ho1-O25	2.361(4)	Er1-O25	2.350(3)	Tm1-O25	2.311(5)
Ho2-O25	2.319(4)	Er2-O25	2.324(3)	Tm2-O25	2.332(5)
Ho3-O25	2.391(4)	Er3-O25	2.369(3)	Tm3-O25	2.312(5)
Ho1-Ho2	3.803(8)	Er1-Er2	3.793(6)	Tm1-Tm2	3.742(7)
Ho1-Ho3	3.896(9)	Er1-Er3	3.874(7)	Tm1-Tm3	3.749(6)
Ho3-Ho2	3.849(8)	Er2-Er3	3.835(6)	Tm2-Tm3	3.756(5)
Ho1-O25-Ho2	108.69(1)	Er1-O25-Er2	108.49(1)	Tm1-O25-Tm2	107.4(2)
Ho1-O25-Ho3	110.17(1)	Er1-O25-Er3	110.34(1)	Tm1-O25-Tm3	108.4(2)
Ho2-O25-Ho3	109.58(1)	Er2-O25-Er3	109.60(1)	Tm2-O25-Tm3	108.0(2)

## Molecular structures of 6-8

Single crystal X-ray diffraction studies reveal that the isomorphous compounds **6-8** crystallize in the triclinic space group,  $P\bar{1}$ . Unlike in compounds **1-5**, the asymmetric unit contains an anionic pentanuclear lanthanide organophosphate unit, with six phosphate ligands, one  $\mu_3$ -OH group at the core, three chelating nitrate groups along with five coordinated methanol and two water molecules. The presence of a half molecule of a doubly protonated cationic ( $\text{tmedaH}_2$ )<sup>2+</sup> group balances the overall charge of the asymmetric unit. In addition to this, there are five non coordinating methanol and two water molecules in the crystal lattice. A perspective view of the molecular structure of compound **6** as a representative example is shown in Figure 7. Compounds **6-8** contain a similar  $\mu_3$ -OH centered metal ion trinuclear unit as seen for **1-5** -  $[\text{Dy}_3(\mu_3\text{-OH})(\text{dipp})_6]$ . The triangular metal ion unit (Dy1-Dy3) is connected to the two peripheral metal ions (Dy4 and Dy5) via the six phosphate ligands. Again the six dipp<sup>2-</sup> ligands display two unique bridging modes -  $[3.111]$  or  $[3.211]$ , again as seen for **1-5**. The average metal oxygen distance in the trinuclear  $[\text{Dy}_3(\mu_3\text{-OH})]$  unit is 2.365 Å, whereas the average metal-metal distance is 3.857 Å. The bridging  $\mu_3$ -OH lies 0.794 Å above the mean plane formed by Dy1, Dy2 and Dy3. The angles around the  $\mu_3$ -OH are in the range of 108.64(1) - 110.24(1)°. The metal-metal distances between the peripheral and the central dysprosium ions vary in the range 5.236-5.605 Å and the metal-metal distance between the peripheral dysprosium ions is 9.833(1) Å. The three nitrate anions chelate to Dy1, Dy4 and Dy5. This differs from **1**, where the nitrates are chelated to the peripheral Nd<sup>III</sup> ions only (Nd4 and Nd5). The coordination of Dy1 is supported solely by chelating nitrate anion and phosphate oxygen atoms unlike in the previous cases (**1-5**). While the coordination number of the central metal ions remain same, that of the peripheral Dy(III) ions are reduced by one with one solvent molecule less (Table S20).

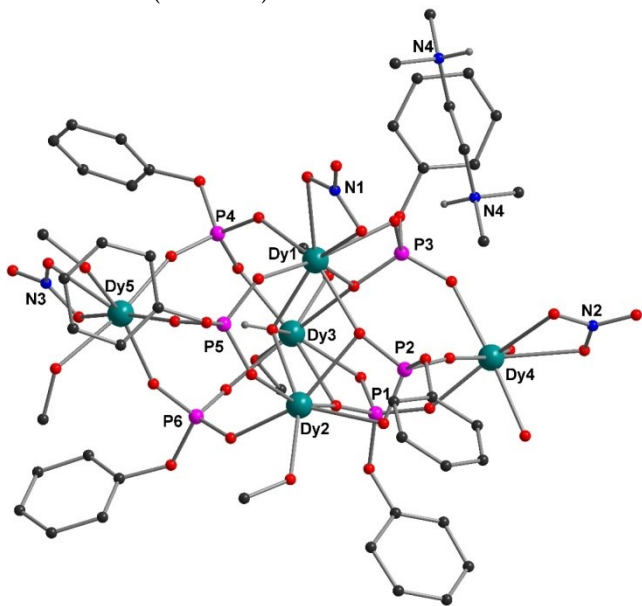


**Figure 7.** Molecular structure of **6** showing the anionic pentanuclear dysprosium organophosphate cluster with the charge balancing protonated cationic tmeda molecule. The full tmeda molecule of the unit cell is shown. Isopropyl

groups, lattice solvates and most hydrogen atoms are removed for clarity.

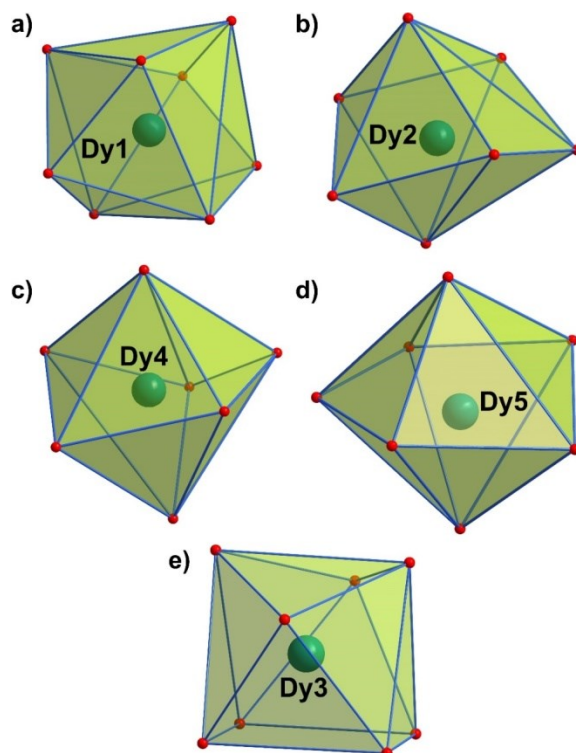


**Figure 8 (a-e).** Distorted coordination geometry around the five Dy(III) ions with ligating oxygen atoms in **6**.

Two Dy(III) ions are eight coordinate and three Dy(III) ions are seven coordinate (Table S17 and S18). This differs from **1-5** where four are eight coordinate and one is seven coordinate. The eight coordinate Dy1 and Dy3 sites adopt distorted triangular dodecahedron and biaugmented trigonal prismatic geometries, respectively. The seven coordinate Dy2 and Dy4 sites display the distorted capped trigonal prismatic environment. Dy5 shows least deviation from the ideal  $D_{5h}$  symmetry showing small distortion from the pentagonal bipyramidal geometry (Figure 8).

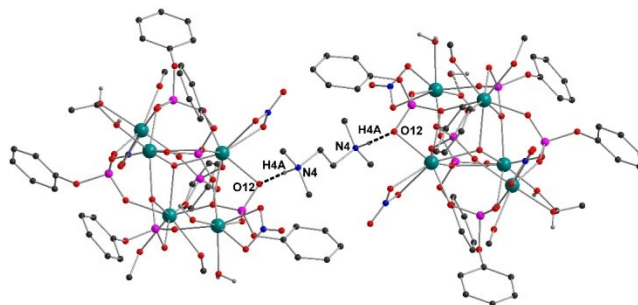


**Figure 9.** The role of the protonated ( $\text{tmedaH}_2$ )<sup>2+</sup> cation in forming H-bonded dimers in **6**.

The doubly protonated ( $\text{tmedaH}_2$ )<sup>2+</sup> molecule facilitates strong intermolecular H-bonding forming a dimer of the pentanuclear rare-earth organophosphate complexes (Figure 9). In addition to the ( $\text{tmedaH}_2$ )<sup>2+</sup> moiety, the coordinated and lattice solvent molecules are also involved in extensive intermolecular and intramolecular H-bonding leading to the formation of two-dimensional self-assembled

hydrogen bonded networks similar to that observed for **1** - **5** (Figure S5).

### Molecular structure of **9**

Unlike **1-8**, compound **9** crystallizes in the monoclinic space group  $P2_1/n$ . The asymmetric part of the unit cell contains five thulium ions, seven doubly deprotonated phosphates, one bridging  $\mu_3$ -OH and coordinated methanol (seven) and water (two) molecules. Contrary to compounds **1-5**, where in addition to the  $\mu_3$ -OH and six  $\text{dipp}^{2-}$  ligands the cationic charge is balanced by two chelating nitrate ions, for **9** the charge is balanced by an extra coordinated  $\text{dipp}^{2-}$  ligand, instead of the two chelating nitrate anions. In addition, there are five non-coordinating methanol and three water molecules present in the lattice. The molecular structure of **9** is depicted in Figure 10, with the same metal ion core observed for **1** - **8**. The average metal-oxygen distance in the trinuclear  $[\text{Tm}_3(\mu_3\text{-OH})(\text{dipp})_6]$  unit is 2.315 Å, whereas the average metal-metal distance is 3.747 Å. The deviation of O25 from the mean plane formed by Tm1, Tm2, and Tm3 is 0.842 Å. Of the seven phosphate ligands present six are bridging and one lies terminal. The six bridging phosphate ligands again bind with the [3.111] or [3.211] modes, whereas the lone terminal phosphate ligand binds in [1.100] mode (Figure 11).<sup>3</sup>The metal-metal distance between the peripheral and central thulium vary over the range 5.315-5.354 Å and the distance between the two peripheral thulium atoms (Tm4 and Tm5) is 9.699 Å.

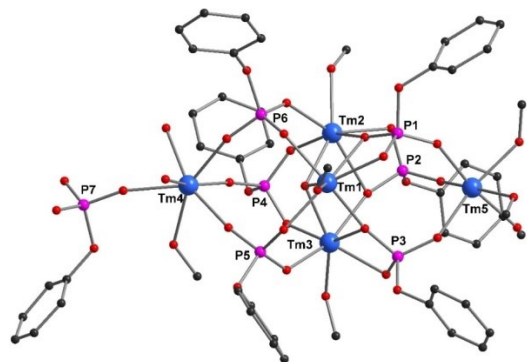


**Figure 10.** Molecular structure of pentanuclear thulium organophosphate **9**. Isopropyl groups, lattice solvates and most hydrogen atoms are removed for clarity.

As we move along the lanthanide series, the coordination number of the thulium ions are further reduced compared to **1** - **8**. Tm1-Tm4 are seven coordinate, while Tm5 is six coordinate (Table S19 and Figure 12). Tm1 displays a distorted capped trigonal prismatic environment, Tm2 and

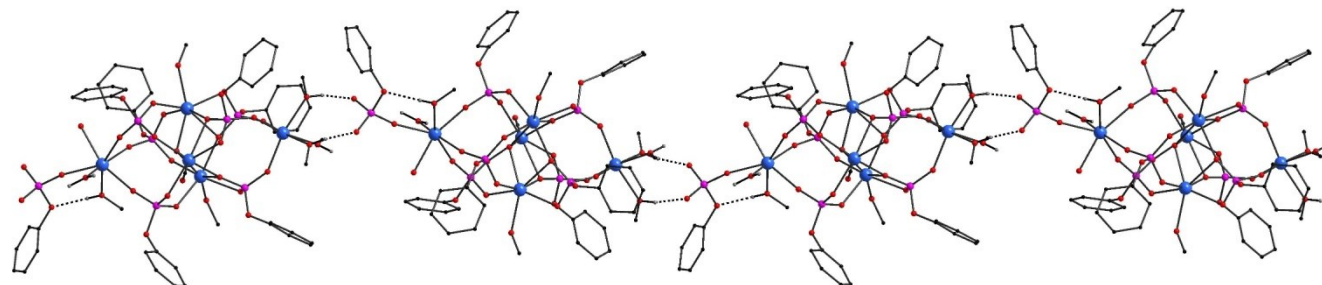


**Figure 13.** Intermolecular H-bonding in **9** leading to the formation of linear polymer of pentanuclear rare-earth phosphate clusters.

Tm3 adopts a pentagonal bipyramidal geometry and Tm4 shows least deviation for the  $C_{3v}$  symmetry with a distorted capped octahedron environment. Tm5 adopts an octahedral geometry, showing least deviation from  $O_h$  symmetry.

Complex **9** forms a one-dimensional chain of pentanuclear units, a consequence of the hydrogen bonding between the terminal phosphate and MeOH/H<sub>2</sub>O groups, in contrast to the two-dimensional sheets formed in the previous examples **1-8** (Figure 13).

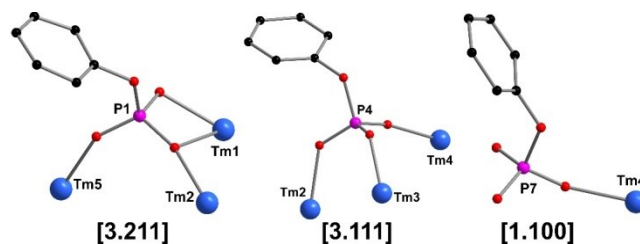


**Figure 11.** Binding modes of the phosphate ligands in **9**.

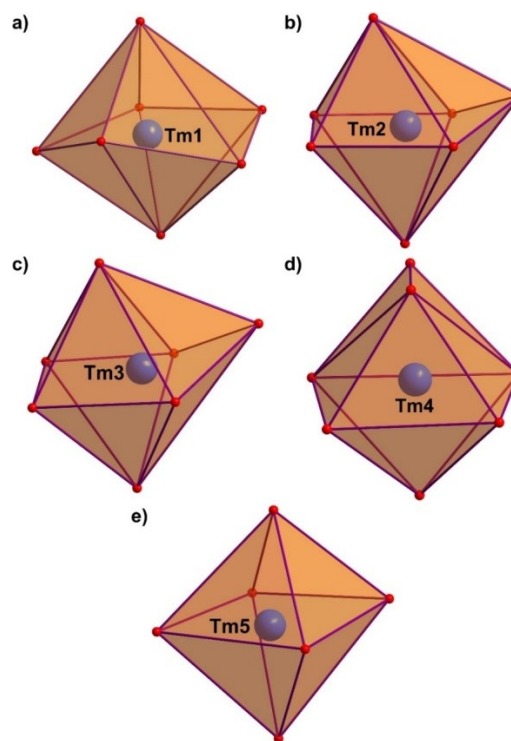


**Figure 12 (a-e).** Polyhedra showing the coordination environment of the five Tm(III) ions in **9**.

## Lanthanide Contraction: Analysis of Ln-( $\mu_3$ -OH) bond lengths and Ln<sub>4</sub>...Ln<sub>5</sub> distances

It is a well-known fact that the ionic radius of Ln(III) ions decrease with increasing atomic number, an effect of weak shielding by f-electrons in the diffused f-orbitals (lanthanide contraction). This effect commonly results in the reduction of the coordination number around the central Ln(III) ion as we move along the series and can also alter the binding mode of the ligand. This, in turn, results in the alteration of the topological structure of the product that results from the reaction. However, apart from the Ln(III) ionic radii, the deviation in structural features across the series also depends on the nature and denticity of the coordinating ligands. In the present scenario, the Ln(III) ions in the pentanuclear lanthanide phosphate compounds **1-9**, show variable coordination numbers ranging from eight to six, decreasing along the series. This can be correlated to the decrease in ionic radii of the respective lanthanide ions with increasing effective nuclear charge. The structural differences in compounds **1-9**, however, impede the evaluation of lanthanide contraction by the quadratic relationship using Slater's model of ionic radii. Although **1-9** are not isomorphous and isostructural due to the varying nature of charge balancing species and coordinating solvent molecules, the average Ln-( $\mu_3$ -OH) bond lengths in the central triangle was considered for examining the decrease in Ln-O bond lengths (Table 3). In Figure 14, the dependence of the average Ln-O<sub>25</sub>( $\mu_3$ -OH) bond length on electronic configuration reveals a steady decrease in the Ln-O distance with increasing atomic number, as one would expect as a consequence of lanthanide contraction. The average Ln-O<sub>25</sub> distance varies in the range 2.467-2.327 Å. The decrease in the Ln-O<sub>25</sub> bond length in turn results in the reduction of Ln...Ln distances within the trinuclear [Ln<sub>3</sub>( $\mu_3$ -OH)(dipp)<sub>6</sub>] unit (Table 3 and Figure 15). Additionally, the combined effect of the decrease in Ln-O bond distances in the pentanuclear lanthanide phosphates results in the decrease of the overall distance between the peripheral Ln(III) ions (Table 3) in the range of 10.266-9.669 Å as depicted in Figure 14. The sudden drop in the Ln<sub>4</sub>...Ln<sub>5</sub> distance after compound **5** is due to the change in the core structure where an additional nitrate anion chelates to one of the Ln(III) ion of the central Ln-O( $\mu_3$ -OH) triangle. Table 3 lists the average Ln-O<sub>25</sub> bond lengths and overall Ln...Ln distances in compounds **1-9**.

**Table 3.** Average Ln-( $\mu_3$ -OH) bond distance and Ln...Ln distances (Å) within the trinuclear [Ln<sub>3</sub>( $\mu_3$ -OH)(dipp)<sub>6</sub>] unit and the distance between the peripheral lanthanide ions (Å) in the pentanuclear lanthanide organophosphate series.

Compound	av. Ln-O <sub>25</sub>	av. Ln...Ln	Ln <sub>4</sub> ...Ln <sub>5</sub>
<b>1</b> (Nd <sup>III</sup> )	2.464	4.017	10.266
<b>2</b> (Sm <sup>III</sup> )	2.433	3.957	10.212
<b>3</b> (Eu <sup>III</sup> )	2.414	3.934	10.184
<b>4</b> (Gd <sup>III</sup> )	2.407	3.915	10.149
<b>5</b> (Tb <sup>III</sup> )	2.397	3.899	10.106
<b>6</b> (Dy <sup>III</sup> )	2.364	3.857	9.834
<b>7</b> (Ho <sup>III</sup> )	2.361	3.849	9.846
<b>8</b> (Er <sup>III</sup> )	2.347	3.834	9.802
<b>9</b> (Tm <sup>III</sup> )	2.323	3.749	9.699

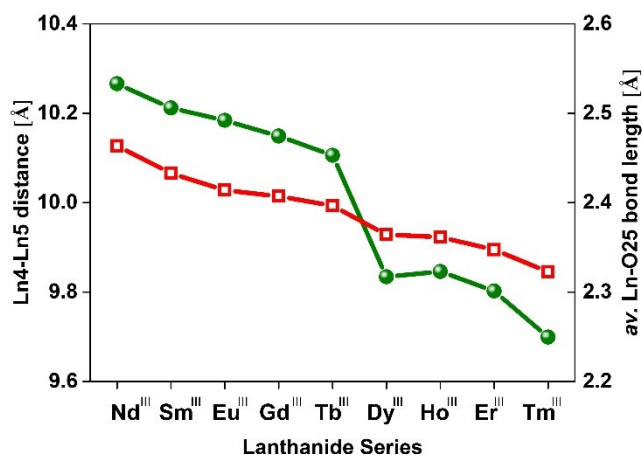


**Figure 14.** Plot of the distance between the peripheral lanthanide ions (Å) and the average Ln-O( $\mu_3$ -OH) bond distance for **1 - 9**, highlighting the effect of lanthanide contraction.

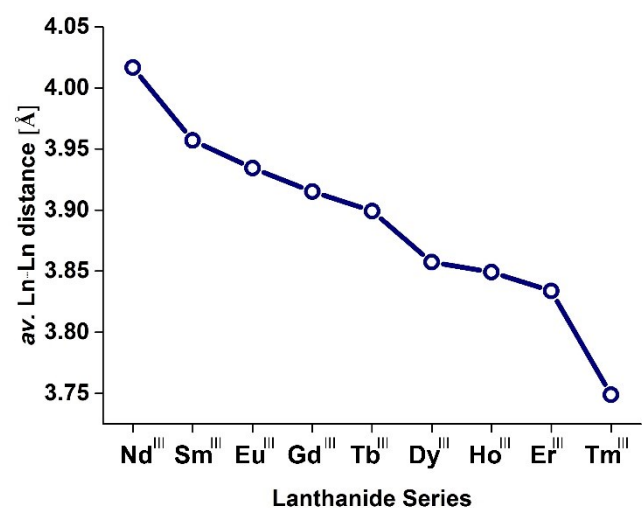


**Figure 15.** Plot of the average Ln-Ln distance in the central triangular unit for **1 - 9**, highlighting the effect of lanthanide contraction.

## Magnetic Properties

Rare-earth metal complexes have played a major role in the advancement of molecular magnetism in the last few years. The magnetic properties of these rare-earth phosphates have been investigated via dc and ac magnetic susceptibility measurements, between 1.8 to 300 K. The dc magnetic susceptibility data were measured with an applied field of 1.0 T in the temperature range 2-300 K. Figures 16 and 17 show the temperature dependence of  $\chi_M T$  ( $\chi_M$  = molar susceptibility) and the field dependence of magnetization of **1-9**, respectively. The expected value for non-interacting Ln<sup>III</sup> ions and the magnetization ( $\mu_B$ ) values at 2 K are presented in Table 4. The  $\chi_M T$  values obtained experimentally for all the complexes are in agreement with calculated values for five non-interacting lanthanide ions at 300 K, except for complex **2** (Sm<sup>III</sup>) (Table 4). The dc susceptibility of the pentanuclear gadolinium cluster, **4**, was reported in the preliminary communication, where the interactions among the Gd<sup>III</sup> ions in the central [Gd<sub>3</sub>( $\mu_3$ -OH)(dipp)<sub>6</sub>] unit and the interaction of the central

**Table 4.** Summary of the static magnetic susceptibility measurement data in  $\text{cm}^3 \text{K mol}^{-1}$ , and effective magnetic moments, in  $\mu_B$ , at 300 K

	4f ion	$2S+1L_J$	Expected $\mu_{\text{eff}}$ values ( $\mu_B$ ) for all ions	Expected $\chi_{\text{M}}T$ value for all ions ( $\text{cm}^3 \text{K mol}^{-1}$ )	Experimental $\mu_{\text{eff}}$ values ( $\mu_B$ )	Experimental $\chi_{\text{M}}T$ value ( $\text{cm}^3 \text{K mol}^{-1}$ )	Magnetization ( $N\mu_B$ ) at 2 K and 5.0 T
1	Nd <sup>III</sup>	$4I_{9/2}$	8.10	8.20	8.21	8.41	7.66
2	Sm <sup>III</sup>	$6H_{5/2}$	1.90	0.45	3.65	1.66	0.36
3	Eu <sup>III</sup>	$7F_0$	0	0	7.37	6.80	0.28
4	Gd <sup>III</sup>	$8S_{7/2}$	17.76	39.40	17.80	39.58	29.62
5	Tb <sup>III</sup>	$7F_6$	21.75	59.05	21.75	59.06	24.72
6	Dy <sup>III</sup>	$6H_{15/2}$	23.83	70.90	23.76	70.47	27.52
7	Ho <sup>III</sup>	$5I_8$	23.74	70.35	23.68	70.03	27.38
8	Er <sup>III</sup>	$4I_{15/2}$	21.44	57.40	21.48	57.64	25.98
9	Tm <sup>III</sup>	$3H_6$	16.92	35.75	17.00	36.07	15.39

Gd<sup>III</sup> ions with the two peripheral ions, both being antiferromagnetic.<sup>8f</sup> The best fit parameters obtained for the pentanuclear gadolinium phosphate cluster were  $J_1 = -0.011 \text{ cm}^{-1}$  and  $J_2 = -0.001 \text{ cm}^{-1}$  (where  $J_1$  is the magnetic exchange interaction among the central  $\text{Gd}_3\text{-O}(\mu_3\text{-OH})$  unit and  $J_2$  is the magnetic exchange interaction between the Gd<sup>III</sup> ions of the central triangle with the peripheral Gd<sup>III</sup> ions). Due to these weak magnetic exchange interactions between the isotropic ions, **4** reveals a significant entropy change ( $-\Delta S_m$ ) of  $25.8 \text{ J kg}^{-1} \text{ K}^{-1}$ , at  $\Delta H = 7 \text{ T}$ .<sup>8f</sup>

The  $\chi_{\text{M}}T$  value of  $8.41 \text{ cm}^3 \text{K mol}^{-1}$  at 300 K for **1** is in good agreement with the expected value for five non-interacting Nd<sup>III</sup> ion ( $S = 3/2, L = 6, J = 9/2, g = 8/11$ ; ground term symbol  $4I_{9/2}$ ) and remains almost constant to 150 K. Further cooling below 150 K shows a gradual decrease in  $\chi_{\text{M}}T$  value reaching a value of  $3.43 \text{ cm}^3 \text{K mol}^{-1}$  at 2 K. The magnetic behavior of anisotropic lanthanide ions is often very complex and difficult to interpret without advanced analysis (theoretical and experimental). The behavior is an interplay of ligand field and spin-orbit effects, which determines a spectrum of  $m_J$  states intrinsically active in Boltzmann population dynamics. It is not a trivial task to determine the energy and nature of such states. For polynuclear complexes magnetic exchange interactions must also be considered, further complicating the analysis. The decrease in the  $\chi_{\text{M}}T$  value as the temperature is reduced is commonly attributed to depopulation of the  $m_J$  magnetic states (i.e. thermal depopulation of the Nd(III) Stark sub levels of the term,  $4I_{9/2}$ ), which is likely the case here, however, the decrease also offers the possibility that antiferromagnetic interactions between the Nd(III) ions are active (dominant). Unfortunately, given the complexity of the system, the profile of the temperature dependence of the magnetic susceptibility cannot be rationalized by “simple” speculation. We can, however, use the data obtained from our analysis of the isotropic  $\{\text{Gd}^{\text{III}}\}_5$  system, complex **4**, which revealed antiferromagnetic interactions between nearest neighbor ions, as a guide. This therefore, indicates that the decrease in the  $\chi_{\text{M}}T$  product is a consequence of single ion thermal depopulation effects and dominant inter-ion antiferromagnetic interactions.

In contrast to **1**, the  $\chi_{\text{M}}T$  value  $1.66 \text{ cm}^3 \text{K mol}^{-1}$  at 300 K for **2** is much higher than that expected for five non-interacting Sm<sup>III</sup> ions ( $S = 5/2, L = 5, J = 5/2, g = 2/7$ ; ground term symbol  $6H_{5/2}$ ), a situation frequently observed in many Sm<sup>III</sup>-based complexes due to the presence of low-lying excited

multiplets.<sup>33</sup> The  $\chi_{\text{M}}T$  value shows a linear dependence on temperature reaching a value of  $0.09 \text{ cm}^3 \text{K mol}^{-1}$  at 2 K.

Compounds **5-9** display similar behavior in the temperature dependence of  $\chi_{\text{M}}T$  values. The experimental  $\chi_{\text{M}}T$  values are in good agreement with the corresponding values for five non-interacting ions (see Table 4). These values gradually decrease, a little, down to  $\sim 50 \text{ K}$  before decreasing sharply on further cooling down to 2 K. The arguments provided for the magnetic behavior of **1** holds true for these anisotropic Tb (**5**), Dy (**6**), Ho (**7**), Er (**8**) and Tm (**9**) ions. We can, again, tentatively conclude from the data that single ion depopulation and antiferromagnetic interactions are responsible for the  $\chi_{\text{M}}T(T)$  profiles. The magnetization versus field data plots for compounds **1-9** (Fig 17), at 2 K, reveal no clear saturation up to a field of 5.0 T, except perhaps for **6** (Dy) which suggests the presence of magnetic anisotropy in these compounds (Figure 17).

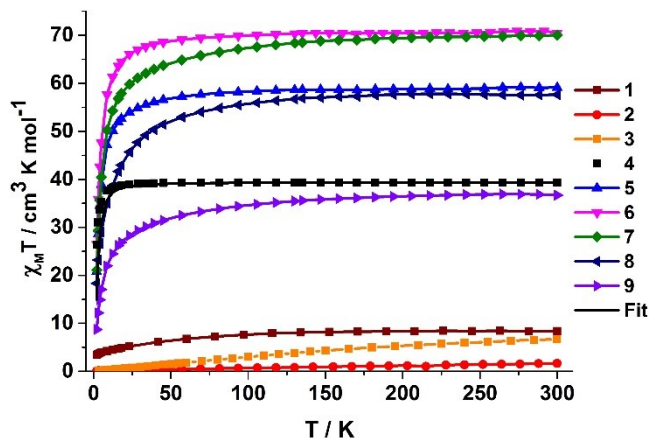


**Figure 16.** Temperature dependence of the  $\chi_{\text{M}}T$  product under an applied field of 1.0 T. (Symbols – experimental points; the black line is the best fit to **4** and coloured lines are guides to the eye).

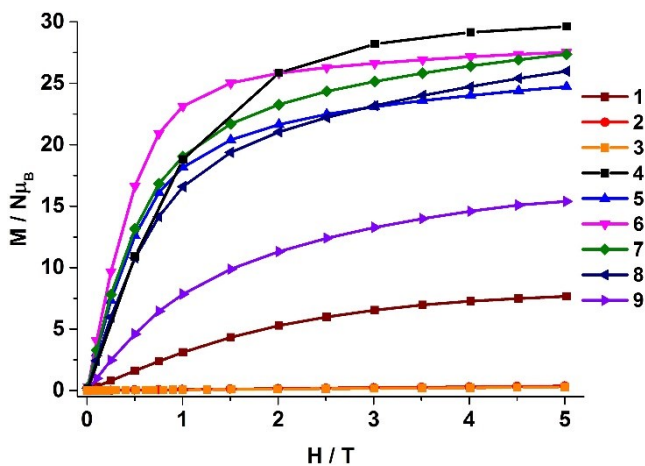


**Figure 17.** Field dependences of the magnetization at 2 K. Solid lines are guides to the eye.

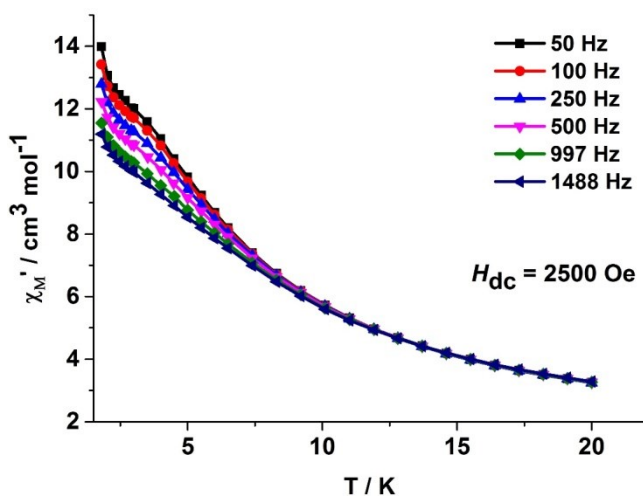


**Figure 18.** Temperature dependence of the real component of the ac susceptibility ( $\chi'$ ) for 6 under an applied dc field of 2500 Oe with a 3.5 Oe oscillating ac field.

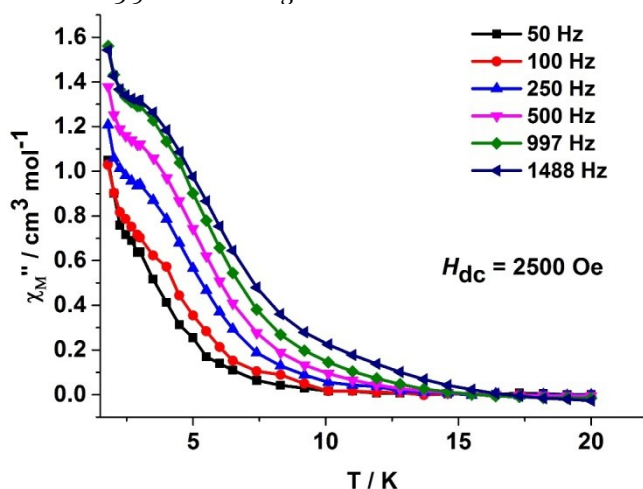


**Figure 19.** Temperature dependence of the imaginary component of the ac susceptibility ( $\chi''$ ) for 6 ( $\text{Dy}^{\text{III}}$ ) under an applied dc field of 2500 Oe with a 3.5 Oe oscillating ac field.

In order to probe for the presence of magnetic anisotropy and SMM behaviour, ac magnetic susceptibility

measurements were carried out. Compounds **1** – **5** and **7** – **9** revealed an absence of out-of-phase susceptibility signals down to 1.8 K, indicating no slow relaxation of the magnetization is observed above this temperature. Compound **6** ( $\text{Dy}^{\text{III}}$ ) on the other hand revealed non-zero out-of-phase ac susceptibility signals ( $\chi''$ ), however no maxima are observed as a function of frequency, (Figure S10). As a consequence, no relaxation times can be extracted. If magnetic relaxation via quantum tunneling of the magnetization (QTM) is active then this relaxation process is generally very fast for lanthanide based complexes, often much faster than the thermally activated process at very low temperatures. The application of an applied field can slow the relaxation time of this process, therefore, allowing for the observation of the thermally activated mechanism. Upon the application of dc field of 2500 Oe, clear temperature dependent out-of-phase ( $\chi''$ ) components of the susceptibility were observed at different frequencies, but the maxima are obscured by a second increase at the lowest temperatures (Figure 19). This behavior clearly indicates the presence of significant QTM, which cannot be quenched even in a 2500 Oe magnetic field. Similar field induced slow magnetic relaxation behavior was observed for **1** and **8** (Figure S8 and S12), again indicating QTM is the most efficient magnetic relaxation mechanism.

We note that a number of pentanuclear lanthanide clusters have been reported recently, containing various numbers of hydroxo bridges and various chelating/bridging ligands, and with core  $\{\text{M}_5\}$  geometries usually different to that seen here. The magnetic behaviors are similar to those described here and some of the reported  $\{\text{Dy}_5\}$  complexes display SMM behavior.<sup>34</sup>

Finally we note that the central triangle  $\{\text{Dy}_3(\mu_3\text{-OH})\}$  in **6** is reminiscent of that in the archetypical single molecule toroidal (SMT) complex  $[\text{Dy}_3(\text{OH})_2(\text{vanillin})_3]$ .<sup>35</sup> There is no evidence of SMT behaviour in **6** with the  $M$  vs  $H$  plot (Figure 17), for example, not showing S-shaped behaviour.

## Conclusions

We have reported the synthesis of a series of pentanuclear lanthanide phosphate complexes derived from the monoester of the phosphoric acid, 2,6-diisopropylidihydrogen phosphate and lanthanide nitrate salts. The molecular structures have been determined by single crystal X-ray diffraction analysis and these compounds have been fully characterized both by analytical and spectroscopic techniques. Compounds **1-8** show extensive H-bonding in the solid-state leading to formation of a 2D sheet of pentanuclear clusters, whereas **9** displays formation of an H-bonded linear polymer. This series of compounds represent the first family of any discrete lanthanide organophosphate complexes using a sterically encumbered phosphate ligand. The effect of the lanthanide contraction was evident from the reduction of the metal ion coordination number and the contraction of the metal-ligand bond length as we moved along the series  $\text{Nd} \rightarrow \text{Tm}$ . Magnetic studies reveal the presence of weak antiferromagnetic magnetic exchange through the bridging  $\mu_3$ -hydroxo and organophosphate ligand for the isotropic  $\{\text{Gd}^{\text{III}}_5\}$  complex. This  $\{\text{Gd}^{\text{III}}_5\}$  cluster revealed a significant entropy change ( $-\Delta S_m$ ) of  $25.8 \text{ J kg}^{-1} \text{ K}^{-1}$ , at  $\Delta H$

= 7 T. The anisotropic lanthanide complexes revealed no clear SMM properties above 2 K due, most likely, to the presence quantum tunneling of magnetization. However, complexes Nd (**1**), Dy (**6**) and Er (**8**) show evidence for slow magnetisation relaxation in applied DC fields.

## Experimental section

### Instruments, methods and materials

All the compounds prepared in this study and the starting materials used are air and moisture stable. Hence all the operations were carried out under aerobic conditions. Solvents were distilled prior to use.<sup>36</sup> Fourier transform infrared spectra were obtained on a Perkin Elmer Spectrum One FT-IR spectrometer as KBr diluted discs. Microanalyses were performed on a ThermoFinnigan (FLASH EA 1112) microanalyzer. Thermogravimetric analysis was carried out on a Perkin Elmer Pyris Diamond TG/DTA analysis system under a stream of nitrogen gas at a heating rate of 10 °C/min. The metal content in the samples were measured by inductively coupled plasma atomic emission spectroscopy (ICP-AES). The samples were digested in nitric acid and diluted with distilled water. The magnetic measurements were carried out on a Quantum Design MPMS-XL SQUID magnetometer equipped with a 7 T magnet. The molar susceptibilities have been calculated using the formulae listed in Table 1. Alternating current (ac) susceptibility measurements were carried out in an oscillating ac field of 3.5 Oe and frequencies ranging from 0.1 to 1500 Hz.

Eu(NO<sub>3</sub>)<sub>3</sub>·5H<sub>2</sub>O, Tb(NO<sub>3</sub>)<sub>3</sub>·xH<sub>2</sub>O, Ho(NO<sub>3</sub>)<sub>3</sub>·6H<sub>2</sub>O, Er(NO<sub>3</sub>)<sub>3</sub>·5H<sub>2</sub>O, Tm(NO<sub>3</sub>)<sub>3</sub>·5H<sub>2</sub>O were procured from Sigma Aldrich. TMEDA was purchased from Spectrochem. Hydrated nitrate salts of neodymium, samarium and dysprosium were prepared by dissolving the corresponding oxides in 50 % aqueous nitric acid and evaporating the solution on a steam bath. 2,6-Di-*iso*-propylphenyl phosphate was synthesized as described previously in the literature.<sup>37</sup>

### X-ray crystallography

Block shaped crystals obtained in the reaction were found to slowly lose transparency when kept outside mother liquor at ambient conditions. Suitable single crystals of each compound were selected and mounted on a Rigaku Saturn 724+ CCD diffractometer, using Paratone oil for unit cell determination and intensity data collection. Data integration and indexing were carried out using Rigaku suite of programs CrystalClear and CrystalStructure.<sup>38</sup> The structures were solved using direct methods (SIR-97).<sup>39</sup> Structure refinement and geometrical calculations were carried out using programs in the WinGX module.<sup>40</sup> The final structure refinement was carried out using full least squares methods on  $F^2$  using SHELXL-2014.<sup>41</sup> The structure refinement details are summarized in Table 5 and 6. Some H-atoms in the solvent molecules could not be refined but their contribution has been included in the molecular formula. Disordered atoms or groups have been handled using PART instructions. In case of **5**, high density peaks around the disordered methanol molecule near Tb5 could not be

modeled and hence left untreated. The diffuse electron density in solvent-accessible regions in **9** was found to be highly disordered and could not be modeled. SQUEEZE procedure of the PLATON program<sup>42</sup> was employed that suggests 273 electrons per unit cell occupying a volume of 1180 Å<sup>3</sup>. This corresponds approximately to two methanol and three water solvates per molecule.

**General procedure for synthesis of compounds 1-9.** To a solution of Ln(NO<sub>3</sub>)<sub>3</sub>·xH<sub>2</sub>O (0.1 mmol) in methanol (10 mL), a solution of dippH<sub>2</sub> (26 mg, 0.1 mmol) in methanol (10 mL) was added. The solution was stirred well and tmeda (23.2 mg, 0.2 mmol) was added to it. The reaction mixture was heated at 60 °C for 2-3 h and then cooled to room temperature. Any solid insoluble portion formed was discarded. The solution was then filtered and the clear filtrate was kept for crystallization at room temperature. The solution was filtered repeatedly until no further precipitation was observed during crystallisation. Crystals from the clear mother liquor was obtained within a period of two-three weeks.

*Characterization of 1.* Yield: 34 mg (72%, based on dippH<sub>2</sub>). M.p: > 250°C. Anal. Calcd. (Found) for C<sub>83</sub>H<sub>157</sub>N<sub>2</sub>Nd<sub>5</sub>O<sub>47</sub>P<sub>6</sub>: C, 35.07 (35.36); H, 5.57 (5.73); N, 0.99 (1.27); Nd, 25.38 (25.57). FT-IR (KBr, cm<sup>-1</sup>): 3574 (s), 3429 (m), 2967 (vs), 2870 (s), 1621 (m), 1467 (s), 1442 (s), 1384 (vs), 1362 (m), 1335 (s), 1256 (s), 1177 (vs), 1143 (vs), 1047 (vs), 1003 (s), 913 (vs), 882 (s), 800 (m), 771 (vs), 748 (s), 662 (s), 599 (s), 544 (s), 520 (s). TGA: Temp. range °C (% Weight loss): 30-111 (5.4); 111-190 (3.9); 190-281 (10.1); 281-801 (29.3).

*Characterization of 2.* Yield: 36.5 mg (76%, based on dippH<sub>2</sub>). M.p: > 250°C. Anal. Calcd. (Found) for C<sub>84</sub>H<sub>159</sub>N<sub>2</sub>O<sub>47</sub>P<sub>6</sub>Sm<sub>5</sub>: C, 34.95 (34.59); H, 5.55 (5.23); N, 0.97 (1.19); Sm, 26.04 (26.18). FT-IR (KBr, cm<sup>-1</sup>): 3577 (s), 3435 (m), 2966 (vs), 2931 (s), 2870 (s), 1621 (s), 1467 (vs), 1441 (vs), 1384 (vs), 1362 (m), 1335 (s), 1256 (s), 1147 (vs), 1047 (s), 1005 (vs), 914 (vs), 882 (s), 800 (m), 770 (vs), 748 (s), 663 (m), 600 (m), 545 (s), 520 (s). TGA: Temp. range °C (% Weight loss): 30-114 (5.3); 114-188 (4.2); 188-272 (9.3); 272-800 (30.0); 800-1000 (2.5).

*Characterization of 3.* Yield: 30 mg (62%, based on dippH<sub>2</sub>). M.p: >250°C. Anal. Calcd. (Found) for C<sub>84</sub>H<sub>159</sub>Eu<sub>5</sub>N<sub>2</sub>O<sub>47</sub>P<sub>6</sub>: C, 34.85 (34.72); H, 5.54 (5.68); N, 0.97 (1.07); Eu, 26.25 (26.52). FT-IR (KBr, cm<sup>-1</sup>): 3589 (s), 3423 (m), 2966 (s), 2869 (m), 1623 (m), 1466 (s), 1440 (s), 1383 (w), 1362 (m), 1336 (s), 1257 (s), 1153 (vs), 1116 (vs), 1047 (s), 1003 (vs), 912 (vs), 880 (m), 770 (vs), 748 (m), 663 (m), 621 (m), 598 (m), 545 (s), 520 (s). TGA: Temp. range °C (% Weight loss): 30-150 (7.5); 150-265 (11.2); 265-408 (27.7); 408-800 (3.3).

*Characterization of 5.* Yield: 27 mg (56%, based on dippH<sub>2</sub>). M.p: > 250°C. Anal. Calcd. (Found) for C<sub>83</sub>H<sub>157</sub>N<sub>2</sub>O<sub>47</sub>P<sub>6</sub>Tb<sub>5</sub>: C, 34.19 (33.80); H, 5.43 (5.66); N, 0.96 (1.23); Tb, 27.25 (27.65). FT-IR (KBr, cm<sup>-1</sup>): 3564 (s), 3418 (s), 3067 (w), 2966 (vs), 2931 (s), 2869 (s), 1622 (m), 1467 (s), 1441 (vs), 1384 (vs), 1362 (m), 1335 (s), 1310 (m), 1256 (s),

1187 (vs), 1155 (vs), 1046 (vs), 1014 (vs), 918 (vs), 882 (s), 800 (m), 768 (vs), 750 (s), 664 (s), 613 (s), 601 (s), 546 (s), 526 (s). TGA: Temp. range °C (% Weight loss): 30-132 (4.2); 132-200 (4.8); 200-274 (7.8); 274-800 (30.2).

**Characterization of 6.** Yield: 41 mg (82%, based on  $\text{dippH}_2$ ). M.p: > 250°C. Anal. Calcd. (Found) for  $\text{C}_{85}\text{H}_{160}\text{Dy}_5\text{N}_4\text{O}_{48}\text{P}_6$ : C, 33.98 (34.36); H, 5.37 (5.63); N, 1.86 (2.27), Dy, 27.04 (27.26). FT-IR (KBr,  $\text{cm}^{-1}$ ): 3558 (s), 3418 (m), 3064 (m), 2966 (vs), 2870 (s), 2626 (m), 2457 (m), 1618 (m), 1465 (s), 1440 (s), 1384 (s), 1335 (s), 1256 (m), 1155 (vs), 1047 (m), 1013 (vs), 916 (s), 882 (m), 800 (m), 770 (s), 749 (s), 663 (m), 600 (s), 546 (s), 523 (s). TGA: Temp. range °C (% Weight loss): 30-102 (2.3); 102-200 (4.4); 200-269 (7.4); 269-800 (32.2).

**Characterization of 7.** Yield: 29 mg (58%, based on  $\text{dippH}_2$ ). M.p: > 250°C. Anal. Calcd. (Found) for  $\text{C}_{85}\text{H}_{160}\text{Ho}_5\text{N}_4\text{O}_{48}\text{P}_6$ : C, 33.84 (34.02); H, 5.35 (5.11); N, 1.86 (2.21), Ho, 27.34 (27.46). FT-IR (KBr,  $\text{cm}^{-1}$ ): 3564 (s), 3434 (m), 2966 (vs), 2931 (s), 2870 (s), 1621 (s), 1467 (vs), 1440 (vs), 1384 (vs), 1362 (s), 1335 (vs), 1256 (s), 1155 (vs), 1047 (vs), 1015 (vs), 917 (vs), 882 (s), 800 (s), 770 (vs), 750 (s), 664 (s), 601 (s), 546 (s), 523 (s), 476 (m). TGA: Temp. range °C (% Weight loss): 30-100 (2.4); 100-199 (4.1); 199-277 (8.4); 277-800 (30.3).

**Characterization of 8.** Yield: 42 mg (84%, based on  $\text{dippH}_2$ ). M.p: > 250°C. Anal. Calcd. (Found) for  $\text{C}_{85}\text{H}_{160}\text{Er}_5\text{N}_4\text{O}_{48}\text{P}_6$ : C, 33.71 (33.80); H, 5.33 (5.39); N, 1.85 (1.47); Er, 27.62 (27.91). FT-IR (KBr,  $\text{cm}^{-1}$ ): 3546 (s), 3401 (m), 2966 (vs), 2870 (vs), 1615 (m), 1468 (s), 1440 (s), 1384 (s), 1335 (s), 1256 (s), 1155 (vs), 1047 (vs), 1015 (vs), 919 (vs), 882 (s), 800 (s), 770 (vs), 750 (s), 664 (s), 630 (s), 601 (s), 547 (s), 523 (s). TGA: Temp. range °C (% Weight loss): 30-100 (2.4); 100-200 (4.7); 200-274 (8.0); 274-800 (31.4).

**Characterization of 9.** Yield: 16 mg (36%, based on  $\text{dippH}_2$ ). M.p: > 250°C. Anal. Calcd. (Found) for  $\text{C}_{96}\text{H}_{178}\text{O}_{46}\text{P}_7\text{Tm}_5$ : C, 36.84 (37.21); H, 5.73 (5.82); Tm, 26.99 (27.26). FT-IR (KBr,  $\text{cm}^{-1}$ ): 3584 (s), 3393 (m), 3067 (m), 2967 (vs), 2870 (s), 1621 (m), 1466 (s), 1440 (s), 1384 (s), 1362 (m), 1336 (s), 1256 (s), 1158 (vs), 1128 (vs), 1047 (s), 1013 (vs), 921 (vs), 799 (m), 800 (m), 770 (vs), 752 (m), 662 (m), 633 (s), 601 (s), 547 (s), 522 (s), 481 (m). TGA: Temp. range °C (% Weight loss): 30-78 (2.9); 78-187 (3.0); 187-251 (9.0); 251-800 (32.8).

## Supporting Information

†Electronic Supplementary Information (SI) available: Synthesis, crystallographic details, additional figures, and spectral characterization. Crystallographic data of **1-3** [CCDC 1520605-1520607] and **5-9** [CCDC 1520608-1520612]. This material is available free of charge via the Internet at <http://pubs.acs.org>.

## AUTHOR INFORMATION

### Corresponding Author

E-mail: [rmv@chem.iitb.ac.in](mailto:rmv@chem.iitb.ac.in)

## Notes

The authors declare no competing financial interest.

## ACKNOWLEDGMENT

This work was supported by (1) DST Nanomission (SR/NM/NS-1119/2011), (2) SERB, New Delhi (SB/S1/IC-48/2013) and (3) IIT-Bombay Bridge Funding. R. M. thanks SERB (SB/S2/JCB-85/2014), for a J. C. Bose Fellowship. S. K. G. thanks UGC for a research fellowship. The authors thank Dr. S. Kuppaswamy, Prof. G. Rajaraman and T. Rajeshkumar for some of the results reported in the preliminary communication of this work. K. S. M. acknowledges receipt of an Australia-India AISRF grant (with G. Rajaraman).

## REFERENCES

- (a) Roy, S.; Chakraborty, A.; Maji, T. K. Lanthanide-organic frameworks for gas storage and as magneto-luminescent materials. *Coord. Chem. Rev.* **2014**, 273-274, 139-164. (b) Shi, F.-N.; Almeida Paz, F. A.; Ribeiro-Claro, P.; Rocha, J. Transposition of chirality from diphosphonate metal-organic framework precursors onto porous lanthanide pyrophosphates. *Chem. Commun.* **2013**, 49, 11668-11670. (c) Ma, S.; Wang, X.-S.; Yuan, D.; Zhou, H.-C. A Coordinatively Linked Yb Metal-Organic Framework Demonstrates High Thermal Stability and Uncommon Gas-Adsorption Selectivity. *Angew. Chem. Int. Ed.* **2008**, 47, 4130-4133. (d) Pan, L.; Adams, K. M.; Hernandez, H. E.; Wang, X.; Zheng, C.; Hattori, Y.; Kaneko, K. Porous Lanthanide-Organic Frameworks: Synthesis, Characterization, and Unprecedented Gas Adsorption Properties. *J. Am. Chem. Soc.* **2003**, 125, 3062-3067.
- (a) Edelmann, F. T. Lanthanide amidinates and guanidinates in catalysis and materials science: a continuing success story. *Chem. Soc. Rev.* **2012**, 41, 7657-7672. (b) Shibasaki, M.; Yoshikawa, N. Lanthanide Complexes in Multifunctional Asymmetric Catalysis. *Chem. Rev.* **2002**, 102, 2187-2210. (c) Weiss, C. J.; Marks, T. J. Organo-f-element catalysts for efficient and highly selective hydroalkoxylation and hydrothiolation. *Dalton Trans.* **2010**, 39, 6576-6588. (d) Trambitas, A. G.; Panda, T. K.; Jenter, J.; Roesky, P. W.; Daniliuc, C.; Hrib, C. G.; Jones, P. G.; Tamm, M. Rare-Earth Metal Alkyl, Amido, and Cyclopentadienyl Complexes Supported by Imidazolin-2-iminato Ligands: Synthesis, Structural Characterization, and Catalytic Application. *Inorg. Chem.* **2010**, 49, 2435-2446. (e) Fadlallah, S.; Terrier, M.; Jones, C.; Roussel, P.; Bonnet, F.; Visseaux, M. Mixed Allyl-Borohydride Lanthanide Complexes: Synthesis of  $\text{Ln}(\text{BH}_4)_2(\text{C}_3\text{H}_5)(\text{THF})_3$  (Ln = Nd, Sm), Characterization, and Reactivity toward Polymerization. *Organometallics* **2016**, 35, 456-461. (f) Arnold, P. L.; McMullon, M. W.; Rieb, J.; Kühn, F. E. C-H Bond Activation by f-Block Complexes. *Angew. Chem. Int. Ed.* **2015**, 54, 82-100.
- (a) Carr, R.; Evans, N. H.; Parker, D. Lanthanide complexes as chiral probes exploiting circularly polarized luminescence. *Chem. Soc. Rev.* **2012**, 41, 7673-7686. (b) Armelao, L.; Quici, S.; Barigelletti, F.; Accorsi, G.; Bottaro, G.; Cavazzini, M.; Tondello, E. Design of luminescent lanthanide complexes: From molecules to highly efficient photo-emitting materials. *Coord. Chem. Rev.* **2010**, 254, 487-505. (c) Galyametdinov, Y. G.; Knyazev, A. A.; Dzhabarov, V. I.; Cardinaels, T.; Driesen, K.; Görlner-Walrand, C.; Binnemans, K. Polarized Luminescence from Aligned Samples of Nematogenic Lanthanide Complexes. *Adv. Mater.* **2008**, 20, 252-257. (d) Zhang, H.; Shan, X.; Zhou, L.; Lin, P.; Li, R.; Ma, E.; Guo, X.; Du, S. Full-colour fluorescent materials based on mixed-lanthanide(iii) metal-organic complexes with high-efficiency white light emission. *J. Mater. Chem. C* **2013**, 1, 888-891. (e) Picot, A.; D'Aléo, A.; Baldeck, P. L.; Grichine, A.; Duperray, A.; Andraud, C.; Maury, O. Long-Lived Two-Photon Excited Luminescence of Water-Soluble Europium Complex: Applications in

- Biological Imaging Using Two-Photon Scanning Microscopy. *J. Am. Chem. Soc.* **2008**, *130*, 1532-1533.
4. (a) New, E. J.; Congreve, A.; Parker, D. Definition of the uptake mechanism and sub-cellular localisation profile of emissive lanthanide complexes as cellular optical probes. *Chem. Sci.* **2010**, *1*, 111-118. (b) Chalmers, K. H.; Kenwright, A. M.; Parker, D.; Blamire, A. M. 19F-lanthanide complexes with increased sensitivity for 19F-MRI: Optimization of the MR acquisition. *Magn. Reson. Med.* **2011**, *66*, 931-936. (c) Hermann, P.; Kotek, J.; Kubicek, V.; Lukes, I. Gadolinium(III) complexes as MRI contrast agents: ligand design and properties of the complexes. *Dalton Trans.* **2008**, 3027-3047.
  5. (a) Peng, H.; Stich, M. I. J.; Yu, J.; Sun, L.-n.; Fischer, L. H.; Wolfbeis, O. S. Luminescent Europium(III) Nanoparticles for Sensing and Imaging of Temperature in the Physiological Range. *Adv. Mater.* **2010**, *22*, 716-719. (b) Shinoda, S.; Tsukube, H. Luminescent lanthanide complexes as analytical tools in anion sensing, pH indication and protein recognition. *Analyst* **2011**, *136*, 431-435. (c) Cui, Y.; Xu, H.; Yue, Y.; Guo, Z.; Yu, J.; Chen, Z.; Gao, J.; Yang, Y.; Qian, G.; Chen, B. A Luminescent Mixed-Lanthanide Metal-Organic Framework Thermometer. *J. Am. Chem. Soc.* **2012**, *134*, 3979-3982.
  6. (a) Layfield, R. A. Organometallic Single-Molecule Magnets. *Organometallics* **2014**, *33*, 1084-1099. (b) Woodruff, D. N.; Winpenny, R. E. P.; Layfield, R. A. Lanthanide Single-Molecule Magnets. *Chem. Rev.* **2013**, *113*, 5110-5148. (c) Rinehart, J. D.; Fang, M.; Evans, W. J.; Long, J. R. A N23- Radical-Bridged Terbium Complex Exhibiting Magnetic Hysteresis at 14 K. *J. Am. Chem. Soc.* **2011**, *133*, 14236-14239. (d) Gregson, M.; Chilton, N. F.; Ariciu, A.-M.; Tuna, F.; Crowe, I. F.; Lewis, W.; Blake, A. J.; Collison, D.; McInnes, E. J. L.; Winpenny, R. E. P.; Liddle, S. T. A monometallic lanthanide bis(methanediide) single molecule magnet with a large energy barrier and complex spin relaxation behaviour. *Chem. Sci.* **2016**, *7*, 155-165. (e) Boulon, M.-E.; Cucinotta, G.; Luzon, J.; Degl'Innocenti, C.; Perfetti, M.; Bernot, K.; Calvez, G.; Caneschi, A.; Sessoli, R. Magnetic Anisotropy and Spin-Parity Effect Along the Series of Lanthanide Complexes with DOTA. *Angew. Chem. Int. Ed.* **2013**, *52*, 350-354. (f) Le Roy, J. J.; Ungur, L.; Korobkov, I.; Chibotaru, L. F.; Murugesu, M. Coupling Strategies to Enhance Single-Molecule Magnet Properties of Erbium-Cyclooctatetraenyl Complexes. *J. Am. Chem. Soc.* **2014**, *136*, 8003-8010.
  7. (a) Gupta, S. K.; Rajeshkumar, T.; Rajaraman, G.; Murugavel, R. An unprecedented zero field neodymium(III) single-ion magnet based on a phosphonic diamide. *Chem. Commun.* **2016**, *52*, 7168-7171. (b) Gupta, S. K.; Rajeshkumar, T.; Rajaraman, G.; Murugavel, R. An air-stable Dy(III) single-ion magnet with high anisotropy barrier and blocking temperature. *Chem. Sci.* **2016**, *7*, 5181-5191. (c) Blagg, R. J.; Ungur, L.; Tuna, F.; Speak, J.; Comar, P.; Collison, D.; Wernsdorfer, W.; McInnes, E. J. L.; Chibotaru, L. F.; Winpenny, R. E. P. Magnetic relaxation pathways in lanthanide single-molecule magnets. *Nat Chem* **2013**, *5*, 673-678. (d) Pugh, T.; Chilton, N. F.; Layfield, R. A. A Low-Symmetry Dysprosium Metallocene Single-Molecule Magnet with a High Anisotropy Barrier. *Angew. Chem. Int. Ed.* **2016**, *55*, 11082-11085. (e) Pugh, T.; Vieru, V.; Chibotaru, L. F.; Layfield, R. A. Magneto-structural correlations in arsenic- and selenium-ligated dysprosium single-molecule magnets. *Chem. Sci.* **2016**, *7*, 2128-2137. (f) Pugh, T.; Tuna, F.; Ungur, L.; Collison, D.; McInnes, E. J. L.; Chibotaru, L. F.; Layfield, R. A. Influencing the properties of dysprosium single-molecule magnets with phosphorus donor ligands. *Nat Commun* **2015**, *6*, 7492.
  8. (a) Zheng, Y.-Z.; Zhou, G.-J.; Zheng, Z.; Winpenny, R. E. P. Molecule-based magnetic coolers. *Chem. Soc. Rev.* **2014**, *43*, 1462-1475. (b) Zheng, Y.-Z.; Evangelisti, M.; Winpenny, R. E. P. Co-Gd phosphonate complexes as magnetic refrigerants. *Chem. Sci.* **2011**, *2*, 99-102. (c) Lorusso, G.; Sharples, J. W.; Palacios, E.; Roubeau, O.; Brechin, E. K.; Sessoli, R.; Rossin, A.; Tuna, F.; McInnes, E. J. L.; Collison, D.; Evangelisti, M. A Dense Metal-Organic Framework for Enhanced Magnetic Refrigeration. *Adv. Mater.* **2013**, *25*, 4653-4656. (d) Evangelisti, M.; Brechin, E. K. Recipes for enhanced molecular cooling. *Dalton Trans.* **2010**, *39*, 4672-4676. (e) Hooper, T. N.; Schnack, J.; Piligkos, S.; Evangelisti, M.; Brechin, E. K. The Importance of Being Exchanged: [Gd<sup>III</sup><sub>4</sub>M<sup>II</sup><sub>8</sub>(OH)<sub>8</sub>(L)<sub>8</sub>(O<sub>2</sub>CR)<sub>8</sub>]<sup>4+</sup> Clusters for Magnetic Refrigeration. *Angew. Chem. Int. Ed.* **2012**, *51*, 4633-4636. (f) Gupta, S. K.; Dar, A. A.; Rajeshkumar, T.; Kuppaswamy, S.; Langley, S. K.; Murray, K. S.; Rajaraman, G.; Murugavel, R. Discrete [Gd<sup>III</sup><sub>4</sub>M] (M = Gd<sup>III</sup> or Co<sup>II</sup>) pentanuclear complexes: a new class of metal-organophosphate molecular coolers. *Dalton Trans.* **2015**, *44*, 5961-5965. (g) Biswas, S.; Mondal, A. K.; Konar, S. Densely Packed Lanthanide Cubane Based 3D Metal-Organic Frameworks for Efficient Magnetic Refrigeration and Slow Magnetic Relaxation. *Inorg. Chem.* **2016**, *55*, 2085-2090. (h) Biswas, S.; Adhikary, A.; Goswami, S.; Konar, S. Observation of a large magnetocaloric effect in a 2D Gd(III)-based coordination polymer. *Dalton Trans.* **2013**, *42*, 13331-13334.
  9. (a) Dorman, J. A.; Choi, J. H.; Kuzmanich, G.; Chang, J. P. High-Quality White Light Using Core-Shell RE<sup>3+</sup>:LaPO<sub>4</sub> (RE = Eu, Tb, Dy, Ce) Phosphors. *J. Phys. Chem. C* **2012**, *116*, 12854-12860. (b) Song, W.-S.; Lee, K.-H.; Do, Y. R.; Yang, H. Utilization of All Hydrothermally Synthesized Red, Green, Blue Nanophosphors for Fabrication of Highly Transparent Monochromatic and Full-Color Plasma Display Devices. *Adv. Funct. Mater.* **2012**, *22*, 1885-1893. (c) Malavasi, L.; Fisher, C. A. J.; Islam, M. S. Oxide-ion and proton conducting electrolyte materials for clean energy applications: structural and mechanistic features. *Chem. Soc. Rev.* **2010**, *39*, 4370-4387. (d) Davis, J. B.; Marshall, D. B.; Morgan, P. E. D. Monazite-containing oxide/oxide composites. *J. Eur. Ceram. Soc.* **2000**, *20*, 583-587. (e) Anfimova, T.; Li, Q.; Jensen, J. O.; Bjerrum, N. J. Thermal stability and proton conductivity of rare earth orthophosphate hydrates. *Int. J. Electrochem. Sci.* **2014**, *9*, 2285-2300. (f) Liu, C.; Hou, Y.; Gao, M. Are Rare-Earth Nanoparticles Suitable for In Vivo Applications? *Adv. Mater.* **2014**, *26*, 6922-6932. (g) Meiser, F.; Cortez, C.; Caruso, F. Biofunctionalization of Fluorescent Rare-Earth-Doped Lanthanum Phosphate Colloidal Nanoparticles. *Angew. Chem. Int. Ed.* **2004**, *43*, 5954-5957. (h) Rao, R. P.; Devine, D. J. RE-activated lanthanide phosphate phosphors for PDP applications. *J. Lumin.* **2000**, *87-89*, 1260-1263.
  10. (a) Hikichi, Y.; Nomura, T. Melting Temperatures of Monazite and Xenotime. *J. Am. Ceram. Soc.* **1987**, *70*, C-252-C-253. (b) Cinibulk, M. K.; Fair, G. E.; Kerans, R. J. High-Temperature Stability of Lanthanum Orthophosphate (Monazite) on Silicon Carbide at Low Oxygen Partial Pressures. *J. Am. Ceram. Soc.* **2008**, *91*, 2290-2297.
  11. Onoda, H.; Tange, K.; Tanaka, I. Influence of lanthanum addition on preparation and powder properties of cobalt phosphates. *J. Mater. Sci.* **2008**, *43*, 5483-5488.
  12. Du, A.; Wan, C.; Qu, Z.; Pan, W. Thermal Conductivity of Monazite-Type REPO<sub>4</sub> (RE=La, Ce, Nd, Sm, Eu, Gd). *J. Am. Ceram. Soc.* **2009**, *92*, 2687-2692.
  13. Ghosh, P.; Oliva, J.; Rosa, E. D. I.; Haldar, K. K.; Solis, D.; Patra, A. Enhancement of Upconversion Emission of LaPO<sub>4</sub>:Er@Yb Core-Shell Nanoparticles/Nanorods. *J. Phys. Chem. C* **2008**, *112*, 9650-9658.
  14. Firsching, F. H.; Brune, S. N. Solubility products of the trivalent rare-earth phosphates. *J. Chem. Eng. Data* **1991**, *36*, 93-95.
  15. Sankar, S.; Nair, B. N.; Suzuki, T.; Anilkumar, G. M.; Padmanabhan, M.; Hareesh, U. N. S.; Warriar, K. G. Hydrophobic and Metallophobic Surfaces: Highly Stable Non-wetting Inorganic Surfaces Based on Lanthanum Phosphate Nanorods. *Sci. Rep.* **2016**, *6*, 22732.
  16. Boakye, E. E.; Mogilevsky, P.; Hay, R. S.; Fair, G. E. Synthesis and Phase Composition of Lanthanide Phosphate Nanoparticles LnPO<sub>4</sub> (Ln=La, Gd, Tb, Dy, Y) and Solid Solutions for Fiber Coatings. *J. Am. Ceram. Soc.* **2008**, *91*, 3841-3849.
  17. Onoda, H.; Nariai, H.; Moriwaki, A.; Maki, H.; Motooka, I. Formation and catalytic characterization of various rare earth phosphates. *J. Mater. Chem.* **2002**, *12*, 1754-1760.
  18. (a) Kitamura, N.; Amezawa, K.; Tomii, Y.; Yamamoto, N. Protonic conduction in rare earth orthophosphates with the monazite structure. *Solid State Ionics* **2003**, *162-163*, 161-165. (b) Amezawa, K.; Tomii, Y.; Yamamoto, N. High temperature protonic conduction in LaPO<sub>4</sub> doped with alkaline earth metals. *Solid State Ionics* **2005**, *176*, 135-141.

19. (a) Riwozki, K.; Meyssamy, H.; Schnablegger, H.; Kornowski, A.; Haase, M. Liquid-Phase Synthesis of Colloids and Redispersible Powders of Strongly Luminescing  $\text{LaPO}_4\text{:Ce,Tb}$  Nanocrystals. *Angew. Chem. Int. Ed.* **2001**, *40*, 573-576. (b) Meyssamy, H.; Riwozki, K.; Kornowski, A.; Nased, S.; Haase, M. Wet-Chemical Synthesis of Doped Colloidal Nanomaterials: Particles and Fibers of  $\text{LaPO}_4\text{:Eu}$ ,  $\text{LaPO}_4\text{:Ce}$ , and  $\text{LaPO}_4\text{:Ce,Tb}$ . *Adv. Mater.* **1999**, *11*, 840-844. (c) Buisette, V.; Moreau, M.; Gacoin, T.; Boilot, J.-P.; Chane-Ching, J.-Y.; Le Mercier, T. Colloidal Synthesis of Luminescent Rhabdophane  $\text{LaPO}_4\text{:Ln}^{3+}\cdot x\text{H}_2\text{O}$  ( $\text{Ln} = \text{Ce, Tb, Eu}$ ;  $x \approx 0.7$ ) Nanocrystals. *Chem. Mater.* **2004**, *16*, 3767-3773.
20. (a) Feigelson, R. S. Synthesis and Single-Crystal Growth of Rare-Earth Orthophosphates. *J. Am. Ceram. Soc.* **1964**, *47*, 257-258. (b) Wang, X.; Gao, M. A facile route for preparing rhabdophane rare earth phosphate nanorods. *J. Mater. Chem.* **2006**, *16*, 1360-1365. (c) Bu, W.; Hua, Z.; Chen, H.; Shi, J. Epitaxial Synthesis of Uniform Cerium Phosphate One-Dimensional Nanocable Heterostructures with Improved Luminescence. *J. Phys. Chem. B* **2005**, *109*, 14461-14464. (d) Bao, J.; Yu, R.; Zhang, J.; Yang, X.; Wang, D.; Deng, J.; Chen, J.; Xing, X. Low-temperature hydrothermal synthesis and structure control of nano-sized  $\text{CePO}_4$ . *CrystEngComm* **2009**, *11*, 1630-1634. (e) Yan, R.; Sun, X.; Wang, X.; Peng, Q.; Li, Y. Crystal Structures, Anisotropic Growth, and Optical Properties: Controlled Synthesis of Lanthanide Orthophosphate One-Dimensional Nanomaterials. *Chem. Eur. J.* **2005**, *11*, 2183-2195. (f) Fang, Y.-P.; Xu, A.-W.; Song, R.-Q.; Zhang, H.-X.; You, L.-P.; Yu, J. C.; Liu, H.-Q. Systematic Synthesis and Characterization of Single-Crystal Lanthanide Orthophosphate Nanowires. *J. Am. Chem. Soc.* **2003**, *125*, 16025-16034.
21. Murugavel, R.; Choudhury, A.; Walawalkar, M. G.; Pothiraja, R.; Rao, C. N. R. Metal Complexes of Organophosphate Esters and Open-Framework Metal Phosphates: Synthesis, Structure, Transformations, and Applications. *Chem. Rev.* **2008**, *108*, 3549-3655.
22. (a) Gupta, S. K.; Kuppaswamy, S.; Walsh, J. P. S.; McInnes, E. J. L.; Murugavel, R. Discrete and polymeric cobalt organophosphates: isolation of a 3-D cobalt phosphate framework exhibiting selective  $\text{CO}_2$  capture. *Dalton Trans.* **2015**, *44*, 5587-5601. (b) Murugavel, R.; Kuppaswamy, S.; Boomishankar, R.; Steiner, A. Hierarchical Structures Built from a Molecular Zinc Phosphate Core. *Angew. Chem. Int. Ed.* **2006**, *45*, 5536-5540. (c) Kalita, A. C.; Gupta, S. K.; Murugavel, R. A Solvent Switch for the Stabilization of Multiple Hemiacetals on an Inorganic Platform: Role of Supramolecular Interactions. *Chem. Eur. J.* **2016**, *22*, 6863-6875. (d) Van Allsburg, K. M.; Anzenberg, E.; Drisdell, W. S.; Yano, J.; Tilley, T. D. Oxygen-Atom Transfer Chemistry and Thermolytic Properties of a Di-tert-Butylphosphate-Ligated  $\text{Mn}_4\text{O}_4$  Cubane. *Chem. Eur. J.* **2015**, *21*, 4646-4654. (e) Ahn, H. S.; Tilley, T. D. Electrocatalytic Water Oxidation at Neutral pH by a Nanostructured  $\text{Co}(\text{PO}_3)_2$  Anode. *Adv. Funct. Mater.* **2013**, *23*, 227-233. (f) Dar, A. A.; Sen, S.; Gupta, S. K.; Patwari, G. N.; Murugavel, R. Octanuclear Zinc Phosphates with Hitherto Unknown Cluster Architectures: Ancillary Ligand and Solvent Assisted Structural Transformations Thereof. *Inorg. Chem.* **2015**, *54*, 9458-9469. (g) Murugavel, R.; Kuppaswamy, S.; Gogoi, N.; Steiner, A.; Bacsá, J.; Boomishankar, R.; Suresh, K. G. Controlling the Structure of Manganese(II) Phosphates by the Choice and Ratio of Organophosphate and Auxiliary Ligands. *Chemistry – An Asian Journal* **2009**, *4*, 143-153.
23. (a) Murugavel, R.; Walawalkar, M. G.; Dan, M.; Roesky, H. W.; Rao, C. N. R. Transformations of Molecules and Secondary Building Units to Materials: A Bottom-Up Approach. *Acc. Chem. Res.* **2004**, *37*, 763-774. (b) Murugavel, R.; Gogoi, N.; Suresh, K. G.; Layek, S.; Verma, H. C. Nuclearity Control in Molecular Iron Phosphates through Choice of Iron Precursors and Ancillary Ligands. *Chem. Asian J.* **2009**, *4*, 923-935. (c) Murugavel, R.; Kuppaswamy, S.; Maity, A. N.; Singh, M. P. Di-, Tri-, Tetra-, and Hexanuclear Copper(II) Mono-organophosphates: Structure and Nuclearity Dependence on the Choice of Phosphorus Substituents and Auxiliary N-Donor Ligands. *Inorg. Chem.* **2009**, *48*, 183-192.
24. (a) Nash, K. L.; Choppin, G. R. Separations Chemistry for Actinide Elements: Recent Developments and Historical Perspective. *Sep. Sci. Technol.* **1997**, *32*, 255-274. (b) Sood, D. D.; Patil, S. K. Chemistry of nuclear fuel reprocessing: Current status. *J. Radioanal. Nucl. Chem.* **1996**, *203*, 547-573. (c) Cocalia, V. A.; Jensen, M. P.; Holbrey, J. D.; Spear, S. K.; Stepinski, D. C.; Rogers, R. D. Identical extraction behavior and coordination of trivalent or hexavalent f-element cations using ionic liquid and molecular solvents. *Dalton Trans.* **2005**, 1966-1971. (d) Paiva, A. P.; Malik, P. Recent advances on the chemistry of solvent extraction applied to the reprocessing of spent nuclear fuels and radioactive wastes. *J. Radioanal. Nucl. Chem.* **2004**, *261*, 485-496. (e) Warf, J. C. Extraction of Cerium(IV) Nitrate by Butyl Phosphate. *J. Am. Chem. Soc.* **1949**, *71*, 3257-3258.
25. (a) Nifant'ev, I. E.; Tavtorkin, A. N.; Shlyahin, A. V.; Korchagina, S. y. A.; Gavrilenko, I. F.; Glebova, N. N.; Churakov, A. V. Easily accessible, hydrocarbon-soluble, crystalline, anhydrous lanthanide (Nd, La, and Y) phosphates. *Dalton Trans.* **2013**, *42*, 1223-1230. (b) Lisowski, J.; Sessler, J. L.; Lynch, V.; Mody, T. D.  $^1\text{H}$  NMR Spectroscopic Study of Paramagnetic Lanthanide(III) Tetrakisphyrins. Effect of Axial Ligation. *J. Am. Chem. Soc.* **1995**, *117*, 2273-2285. (c) Zeng, G.; Guo, X.; Wang, C.; Lin, Y.; Li, H. Crystal structure of tris(dimethyl phosphato)lanthanum(III) coordination polymer  $[\text{La}(\text{PO}_2(\text{OCH}_3)_2)_3]_n$ . *Jiegou Huaxue* **1994**, *3*, 24. (d) Li, L.; Lin, Y.; Zeng, G.; Ma, A. Synthesis and crystal structure of complex of samarium with dimethyl phosphate. *Yingyong Huaxue* **1989**, *6*, 53-57. (e) Li, L.; Lin, Y.; Zeng, G.; Ma, A. Synthesis and crystal structure of tris(dimethyl phosphate)europium. *Jiegou Huaxue* **1991**, *10*, 155-158. (f) Ma, A.; Li, L.; Lin, Y.; Zeng, G.; Li, H. Synthesis and structural study of praseodymium-dimethyl phosphate complex. *Zhongguo Xitu Xuebao* **1990**, *8*, 201-204. (g) Liu, C.; Wu, G.; Tang, Z.; Han, Y.; Pan, Z.; Shi, N.; Liao, L. Synthesis and crystal structure of lanthanum dimethyl phosphate monohydrate. **1990**, *48*, 116-120. (h) Ma, A.; Li, L.; Lin, Y.; Zeng, G.; Jin, S.; Li, H. Synthesis and crystal structure of lanthanum complex with tris(dimethyl phosphate) and trimethyl phosphate. *Yingyong Huaxue* **1989**, *6*, 99-103. (i) Han, Y.; Pan, Z.; Shi, N.; Liao, L.; Liu, C.; Wu, G.; Tang, Z.; Xiao, Y. Crystal structures of cerium and praseodymium diethylphosphates. *Wuji Huaxue Xuebao* **1990**, *6*, 17-24. (j) Huang, C.; Yi, T.; Lu, Y.; Xu, G.; Ling, H.; Ma, Z. Crystal structures of cerium and praseodymium diethylphosphates. *Chin. Chem. Lett.* **1992**, *3*, 947-950. (k) Lebedev, V. G.; Palkina, K. K.; Maksimova, S. I.; Lebedeva, E. N.; Galaktionova, O. V. Z. Synthesis and structure of tris(diethyl phosphate)neodymium crystals. *Z. Neorg. Khim.* **1982**, *27*, 2980-2982.
26. (a) Mokry, L. M.; Dean, N. S.; Carrano, C. J. Synthesis and Structure of a Discrete Hexanuclear Uranium-Phosphate Complex. *Angew. Chem. Int. Ed. Engl.* **1996**, *35*, 1497-1498. (b) Burns, J. H. Solvent-extraction complexes of the uranyl ion. 2. Crystal and molecular structures of catena-bis( $\mu$ -di-n-butyl phosphato-O,O')dioxouranium(VI) and bis( $\mu$ -di-n-butyl phosphato-O,O')bis[(nitrato)(tri-n-butylphosphine oxide)dioxouranium(VI)]. *Inorg. Chem.* **1983**, *22*, 1174-1178. (c) Kanellakopoulos, B.; Dernberger, E.; Maier, R.; Nuber, B.; Stammler, H.-G.; Ziegler, M. L. Molecular structure and charge distribution. IV. Electric dipole moment of the 1:2 adducts of uranyl nitrate with trialkyl phosphates. The crystal structure of  $\text{UO}_2(\text{TEP})_2(\text{NO}_3)_2$  and bis[(m-diethyl phosphato-O,O')nitrato(triethyl phosphate)dioxouranium(VI)],  $\{(\text{UO}_2)[(\text{EtO})_2\text{PO}_2][(\text{EtO})_3\text{PO}](\text{NO}_3)_2\}_z$ . *Z. Anorg. Allg. Chem.* **1993**, *619*, 593-600.
27. (a) Zheng, Y.-Z.; Evangelisti, M.; Tuna, F.; Winpenny, R. E. P. Co-Ln Mixed-Metal Phosphonate Grids and Cages as Molecular Magnetic Refrigerants. *J. Am. Chem. Soc.* **2012**, *134*, 1057-1065. (b) Sheikh, J. A.; Clearfield, A. Heterometallic CoIII-GdIII Clusters as Magnetic Refrigerants. *Inorg. Chem.* **2016**, *55*, 8254-8256. (c) Zheng, Y.-Z.; Pineda, E. M.; Helliwell, M.; Winpenny, R. E. P.  $\text{Mn}^{\text{II}}\text{-Gd}^{\text{III}}$  Phosphonate Cages with a Large Magnetocaloric Effect. *Chem. Eur. J.* **2012**, *18*, 4161-4165. (d) Tang, X.; Xu, Y.; Ye, W.; Tang, Y.; Ma, Y.; Yuan, R.  $\text{Mn}(\text{II})_2\text{Gd}(\text{III})_3$  Phosphonate as a Molecular Refrigerant. *Aust. J. Chem.* **2015**, *68*, 1926-1928. (e) Moreno Pineda, E.; Tuna, F.; Pritchard,

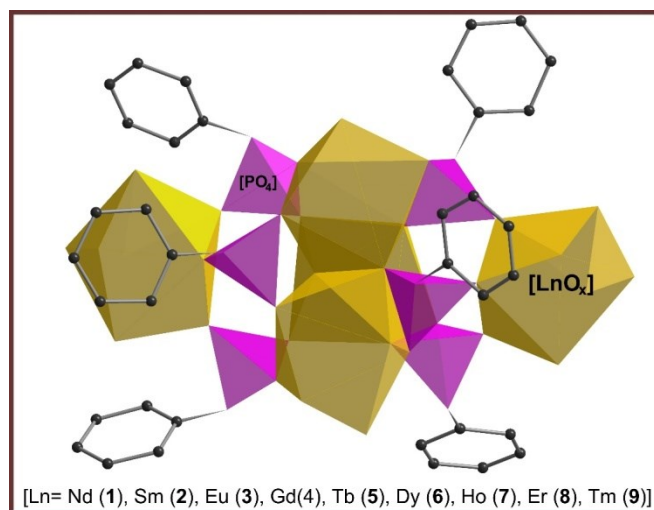
- R. G.; Regan, A. C.; Winpenny, R. E. P.; McInnes, E. J. L. Molecular amino-phosphonate cobalt-lanthanide clusters. *Chem. Commun.* **2013**, 49, 3522-3524. (f) Tang, X.; Zhong, Q.; Xu, J.; Li, H.; Xu, S.; Cui, X.; Wei, B.; Ma, Y.; Yuan, R. Co(II)<sub>4</sub>Gd(III)<sub>6</sub> phosphonate grid and cage as molecular refrigerants. *Inorg. Chim. Acta* **2016**, 442, 195-199. (g) Pineda, E. M.; Tuna, F.; Zheng, Y.-Z.; Winpenny, R. E. P.; McInnes, E. J. L. Wells-Dawson Cages as Molecular Refrigerants. *Inorg. Chem.* **2013**, 52, 13702-13707.
28. (a) Raganathan, K. G.; Schneider, H.-J. Binuclear Lanthanide Complexes as Catalysts for the Hydrolysis of Bis(p-nitrophenyl)-phosphate and Double-Stranded DNA. *Angew. Chem. Int. Ed. Engl.* **1996**, 35, 1219-1221. (b) Yoo, B.; Pagel, M. Lanthanide-Mediated Dephosphorylation Used for Peptide Cleavage during Solid Phase Peptide Synthesis. *Molecules* **2013**, 18, 3894. (c) Aguilar-Pérez, F.; Gómez-Tagle, P.; Collado-Fregoso, E.; Yatsimirsky, A. K. Phosphate Ester Hydrolysis by Hydroxo Complexes of Trivalent Lanthanides Stabilized by 4-Imidazolecarboxylate. *Inorg. Chem.* **2006**, 45, 9502-9517. (d) Roigk, A.; Yescheulova, O. V.; Fedorov, Y. V.; Fedorova, O. A.; Gromov, S. P.; Schneider, H.-J. Carboxylic Groups as Cofactors in the Lanthanide-Catalyzed Hydrolysis of Phosphate Esters. Stabilities of Europium(III) Complexes with Aza-benzo-15-crown-5 Ether Derivatives and Their Catalytic Activity vs Bis(p-nitrophenyl)phosphate and DNA. *Org. Lett.* **1999**, 1, 833-835. (e) Roigk, A.; Hettich, R.; Schneider, H.-J. Unusual Catalyst Concentration Effects in the Hydrolysis of Phenyl Phosphate Esters and of DNA: A Systematic Investigation of the Lanthanide Series. *Inorg. Chem.* **1998**, 37, 751-756.
29. (a) Murugavel, R.; Gogoi, N.; Clérac, R. Tetra- and Decanuclear Iron(III) Phosphonates: Observance of a Rare P-C Bond Cleavage in a Homogeneous Medium. *Inorg. Chem.* **2009**, 48, 646-651. (b) Goura, J.; Walsh, J. P. S.; Tuna, F.; Halder, R.; Maji, T. K.; Chandrasekhar, V. P-C Bond Cleavage-Assisted Lanthanide Phosphate Coordination Polymers. *Cryst. Growth Des.* **2015**, 15, 2555-2560.
30. (a) Li, X.; Sun, H.-L.; Wu, X.-S.; Qiu, X.; Du, M. Unique (3,12)-Connected Porous Lanthanide-Organic Frameworks Based on Ln<sub>4</sub>O<sub>4</sub> Clusters: Synthesis, Crystal Structures, Luminescence, and Magnetism. *Inorg. Chem.* **2010**, 49, 1865-1871. (b) Baskar, V.; Roesky, P. W. Lanthanide hydroxide cubane clusters anchoring ferrocenes: model compounds for fixation of organometallic fragments on a lanthanide oxide surface. *Dalton Trans.* **2006**, 676-679. (c) Zhou, J.-M.; Shi, W.; Li, H.-M.; Li, H.; Cheng, P. Experimental Studies and Mechanism Analysis of High-Sensitivity Luminescent Sensing of Pollutational Small Molecules and Ions in Ln<sub>4</sub>O<sub>4</sub> Cluster Based Microporous Metal-Organic Frameworks. *J. Phys. Chem. C* **2014**, 118, 416-426. (d) Ma, B.-Q.; Zhang, D.-S.; Gao, S.; Jin, T.-Z.; Yan, C.-H.; Xu, G.-X. From Cubane to Supercubane: The Design, Synthesis, and Structure of a Three-Dimensional Open Framework Based on a Ln<sub>4</sub>O<sub>4</sub> Cluster. *Angew. Chem.* **2000**, 112, 3790-3792.
31. Coxall, R. A.; Harris, S. G.; Henderson, D. K.; Parsons, S.; Tasker, P. A.; Winpenny, R. E. P. Inter-ligand reactions: in situ formation of new polydentate ligands. *Journal of the Chemical Society, Dalton Transactions* **2000**, 2349-2356.
32. Llunell, M.; Casanova, D.; Cirera, J.; Bofill, J.; Alemany, P.; Alvarez, S. SHAPE (Version 2.1), Barcelona, 2013.
33. (a) Chakraborty, J.; Ray, A.; Pilet, G.; Chastanet, G.; Luneau, D.; Ziessel, R. F.; Charbonniere, L. J.; Carrella, L.; Rentschler, E.; El Fallah, M. S.; Mitra, S. Syntheses, characterisation, magnetism and photoluminescence of a homodinuclear Ln(III)-Schiff base family. *Dalton Trans.* **2009**, 10263-10272. (b) Zhao, L.; Lin, S.; Shen, S.; Tang, J. A novel two dimensional samarium(III) coordination framework with N-(2-Hydroxyethyl)iminodiacetic acid and oxalate ligands: Synthesis, crystal structure and magnetic property. *Inorg. Chem. Commun.* **2011**, 14, 1928-1931. (c) Yang, X.-D.; Zhang, C.-H.; Wang, D.-P.; Chen, Y.-G. A new 2D network constructed by polymeric anions and lanthanides. Synthesis, structure and magnetic property of two new compounds. *Inorg. Chem. Commun.* **2010**, 13, 1350-1353.
34. (a) Ge, J.-Y.; Ru, J.; Gao, F.; Song, Y.; Zhou, X.-H.; Zuo, J.-L. Pentanuclear lanthanide pyramids based on thiacalix[4]arene ligand exhibiting slow magnetic relaxation. *Dalton Trans.* **2015**, 44, 15481-15490. (b) Gamer, M. T.; Lan, Y.; Roesky, P. W.; Powell, A. K.; Clérac, R. Pentanuclear Dysprosium Hydroxy Cluster Showing Single-Molecule-Magnet Behavior. *Inorg. Chem.* **2008**, 47, 6581-6583. (c) Andrews, P. C.; Beck, T.; Fraser, B. H.; Junk, P. C.; Massi, M.; Moubaraki, B.; Murray, K. S.; Silberstein, M. Functionalised β-diketonate polynuclear lanthanoid hydroxo clusters: Synthesis, characterisation, and magnetic properties. *Polyhedron* **2009**, 28, 2123-2130. (d) Zhang, Z.; Zhang, Y.; Zheng, Z. In *Recent Development in Clusters of Rare Earths and Actinides: Chemistry and Materials*; Zheng, Z., Ed.; Springer Berlin Heidelberg: Berlin, Heidelberg, 2017; pp 1-49.
35. (a) Chibotaru, L. F.; Ungur, L.; Soncini, A. The Origin of Nonmagnetic Kramers Doublets in the Ground State of Dysprosium Triangles: Evidence for a Toroidal Magnetic Moment. *Angew. Chem. Int. Ed.* **2008**, 47, 4126-4129. (b) Li, X.-L.; Wu, J.; Tang, J.; Le Guennic, B.; Shi, W.; Cheng, P. A planar triangular Dy<sub>3</sub> + Dy<sub>3</sub> single-molecule magnet with a toroidal magnetic moment. *Chem. Commun.* **2016**, 52, 9570-9573.
36. Armarego, W. L. F.; Perrin, D. D. Purification of laboratory chemicals, Butterworth Heinemann, Oxford, Boston 1996.
37. Kosolapoff, G. M.; Arpke, C. K.; Lamb, R. W.; Reich, H. Structural effects in reactions of organophosphorus compounds. I. Reactions of phosphorus oxychloride with hindered phenols. *J. Chem. Soc. C* **1968**, 815-818.
38. CrystalClear, V.-S. E. r., 2009 and CrystalStructure, Version 4.0. Rigaku, 2010.
39. Altomare, A.; Burla, M. C.; Camalli, M.; Cascarano, G. L.; Giacovazzo, C.; Guagliardi, A.; Moliterni, A. G. G.; Polidori, G.; Spagna, R. SIR97: a new tool for crystal structure determination and refinement. *J. Appl. Crystallogr.* **1999**, 32, 115-119.
40. Farrugia, L. WinGX and ORTEP for Windows: an update. *J. Appl. Crystallogr.* **2012**, 45, 849-854.
41. Sheldrick, G. Crystal structure refinement with SHELXL. *Acta Crystallographica Section C* **2015**, 71, 3-8.
42. Spek, A. Single-crystal structure validation with the program PLATON. *J. Appl. Crystallogr.* **2003**, 36, 7-13.

**Table 5.** Data Collection and Structure Refinement details for 1-5.

Compound	1	2	3	5
CCDC	1520605	1520606	1520607	1520608
Identification code	SKG420	SKG421	SKG424	SKG546R
Empirical Formula	C <sub>83</sub> H <sub>157</sub> N <sub>3</sub> Nd <sub>5</sub> O <sub>47</sub> P <sub>6</sub>	C <sub>84</sub> H <sub>159</sub> Sm <sub>5</sub> N <sub>2</sub> O <sub>47</sub> P <sub>6</sub>	C <sub>84</sub> H <sub>159</sub> Eu <sub>5</sub> N <sub>2</sub> O <sub>47</sub> P <sub>6</sub>	C <sub>83</sub> H <sub>157</sub> N <sub>2</sub> O <sub>47</sub> P <sub>6</sub> Tb <sub>3</sub>
Temp. (K)	150(2)	150(2)	150(2)	150(2)
Crystal system	Triclinic	Triclinic	Triclinic	Triclinic
Space group	<i>P</i> -1	<i>P</i> -1	<i>P</i> -1	<i>P</i> -1
a (Å)	14.219(2)	14.157(2)	14.125(3)	14.124(2)
b (Å)	17.081(3)	17.015(3)	16.970(4)	16.848(3)
c (Å)	25.463(4)	25.380(4)	25.374(5)	25.418(4)
α (°)	99.330(2)	99.338(3)	99.462(3)	99.442(3)
β (°)	90.523(3)	90.6540(10)	90.702(3)	90.785(3)
γ (°)	105.789(3)	105.732(4)	105.645(4)	105.199(3)
Volume (Å <sup>3</sup> )	5863.0(16)	5796.7(16)	5767(2)	5747.6(16)
Z	2	2	2	2
μ (mm <sup>-1</sup> )	2.339	2.660	2.847	3.208
Crystal size (mm <sup>3</sup> )	0.20 x 0.18 x 0.10	0.12 x 0.10 x 0.04	0.15 x 0.13 x 0.08	0.24 x 0.16 x 0.16
Reflections collected	43876	43224	43281	42877
Independent reflections	20432 [R(int) = 0.0378]	20130 [R(int) = 0.0304]	20070 [R(int) = 0.0250]	19999 [R(int) = 0.0275]
Data / restraints / parameters	20432 / 22 / 1309	20130 / 34 / 1344	20070 / 19 / 1381	19999 / 1394 / 1398
Goodness-of-fit on F <sup>2</sup>	1.073	1.124	1.076	1.128
Final R indices [I > 2σ(I)]	R1 = 0.0479, wR2 = 0.1170	R1 = 0.0425, wR2 = 0.0956	R1 = 0.0316, wR2 = 0.0780	R1 = 0.0424, wR2 = 0.1034
R indices (all data)	R1 = 0.0493, wR2 = 0.1181	R1 = 0.0440, wR2 = 0.0968	R1 = 0.0326, wR2 = 0.0787	R1 = 0.0432, wR2 = 0.1039
Largest diff. peak and hole (e.Å <sup>-3</sup> )	3.377 and -2.940	2.968 and -1.902	2.525 and -1.356	3.664 and -2.159

**Table 6.** Data Collection and Structure Refinement details for 6-9.

Compound	6	7	8	9
CCDC	1520609	1520610	1520611	1520612
Identification code	SKG422	SKG586	SKG427	SKG620
Empirical Formula	C <sub>85</sub> H <sub>160</sub> Dy <sub>5</sub> N <sub>4</sub> O <sub>48</sub> P <sub>6</sub>	C <sub>85</sub> H <sub>160</sub> Ho <sub>5</sub> N <sub>4</sub> O <sub>48</sub> P <sub>6</sub>	C <sub>85</sub> H <sub>160</sub> Er <sub>5</sub> N <sub>4</sub> O <sub>48</sub> P <sub>6</sub>	C <sub>96</sub> H <sub>178</sub> O <sub>46</sub> P <sub>7</sub> Tm <sub>5</sub>
Temp. (K)	150(2)	150(2)	150(2)	150(2)
Crystal system	Triclinic	Triclinic	Triclinic	Monoclinic
Space group	<i>P</i> -1	<i>P</i> -1	<i>P</i> -1	<i>P</i> <sub>2</sub> / <i>n</i>
a (Å)	15.213(2)	15.264(4)	15.253(3)	14.8572(16)
b (Å)	15.987(2)	15.993(4)	16.025(3)	34.890(4)
c (Å)	26.093(4)	26.040(6)	26.013(5)	24.726(3)
α (°)	94.125(2)	93.585(4)	93.779(3)	90
β (°)	99.124(3)	99.456(3)	99.260(2)	90.716(2)
γ (°)	106.545(2)	106.490(3)	106.619(2)	90
Volume (Å <sup>3</sup> )	5960.2(14)	5972(3)	5971(2)	12816(3)
Z	2	2	2	4
μ (mm <sup>-1</sup> )	3.261	3.438	3.640	3.586
Crystal size (mm <sup>3</sup> )	0.21 x 0.19 x 0.13	0.13 x 0.12 x 0.07	0.15 x 0.10 x 0.08	0.20 x 0.20 x 0.16
Reflections collected	44056	44551	44898	76915
Independent reflections	20642 [R(int) = 0.0260]	20667 [R(int) = 0.0398]	20785 [R(int) = 0.0326]	22993 [R(int) = 0.0912]
Data / restraints / parameters	20642 / 21 / 1426	20667 / 32 / 1432	20785 / 18 / 1410	22993 / 51 / 1388
Goodness-of-fit on F <sup>2</sup>	1.07	1.115	1.0069	1.105
Final R indices [I > 2σ(I)]	R1 = 0.0298, wR2 = 0.0737	R1 = 0.0412, wR2 = 0.0984	R1 = 0.0384, wR2 = 0.0911	R1 = 0.0531, wR2 = 0.1263
R indices (all data)	R1 = 0.0309, wR2 = 0.0747	R1 = 0.0430, wR2 = 0.1004	R1 = 0.0404, wR2 = 0.0929	R1 = 0.0656, wR2 = 0.1291
Largest diff. peak and hole (e.Å <sup>-3</sup> )	1.815 and -2.053	1.627 and -2.108	2.185 and -1.405	1.822 and -1.155



The present study describes a series of primary structurally characterized pentanuclear rare-earth organophosphates  $[\text{Ln}_5(\mu_3\text{-OH})(\text{dipp})_6(\text{CH}_3\text{OH})_x(\text{H}_2\text{O})_y]^{2+}$  [Ln= Nd (1), Sm (2), Eu (3), Gd (4), Tb (5), Dy (6), Ho (7), Er (8), Tm (9)] assembled from a sterically encumbered mono-ester of phosphoric acid under mild reaction conditions. The magnetic properties are described. Insights into the structure make the effect of the lanthanide contraction evident from the reduction in the coordination number around Ln ions and shortening of Ln-O bonds.